Review on "Comparison of vertical aerosol extinction coefficients from in-situ and LIDAR measurements"/"Comparison of aerosol extinction coefficients as retrieved from in-situ measurements and elastic back-scatter LIDAR"

Our answers to the comments are given below in blue letters, while the referee comments are given in *black italics*. Additionally, we added the changes we made in the revised manuscript in **blue bold** letters.

Reply to Referee #1:

After the review I think that the manuscript still presents some questions that need to be solved. The main question is that of the retrieval of aerosol extinction coefficient with elastic backscatter LIDAR. After considering my comments and those of the other reviewer the authors improve the manuscript. Nevertheless, as far as they use the in-situ information for estimating a Lidar Ratio the idea of independent comparison between extinction retrieved from in-situ and backscatter LIDAR fails. In this sense, I suggest a change in the focus of the manuscript that will be reflected in the new proposed tittle: "Studying the vertical aerosol extinction coefficient by combination of in-situ and elastic backscatter LIDAR". As far as the authors consider this change, including the appropriate modifications of the manuscript in order to focus in this aspect, I think that the concern on the retrieval of extinction coefficient profiles from elastic backscatter LIDAR will be solved.

Following the referee's request we calculated LIDAR ratios (LR) using in-situ data combined with Mie-codes and included them in the revised manuscript. However, it is very crucial to note that these values were not used for any further calculations or retrievals! They simply serve as a comparison to literature-LR values, helping us to understand and evaluate whether the literature-LRs make sense for our study. In our analysis we used LRs presented in the literature (e.g. 30, 50 and 70sr) in order to be able to compare results from two independent methods.

For this reason, we propose to change the suggested title to **"Studying the vertical aerosol extinction coefficient by comparing in-situ airborne data and elastic back-scatter LIDAR".**

To clarify the use of the calculated LIDAR ratios we added the following passages to the manuscript:

Added and revised text: Page: 18624; line 3:

Table 1 shows a list of LR used in our inversion, classified according to *R*, DR and altitude. The Po Valley aerosol is predominantly of continental origin and therefore LR values between 30 and 70 sr seem to fit best as found using the CALIPSO model by Omar et al. (2009) for clean and polluted continental aerosol particles, respectively, both at λ=532 nm. These values agree well with model results for continental aerosol presented by Barnaba and Gobbi (2004) who found LR values of 60 sr. Measurements performed in Southern Italy found LR values of approximately 50 sr below 2 km at a wavelength of 351 nm (Pisani, 2006; De Tomasi et al., 2006). Discrepancies in LR may arise from the selected method to retrieve it and from the exact location. For instance, Müller et al. (2007) showed that comparing elastic LIDAR against AERONET sun photometers generally yields higher LR compared

to LR directly from Raman LIDARS. In order to evaluate the LR assumption from literature data, we performed Mie calculations for the back-scatter coefficients using the airborne in-situ data. By applying Eq. (11) the in-situ derived LR was calculated and yielded values between 51-67 sr, with a mean value of 58 ± 4 sr. These results indicate that the range of LIDAR values, which were chosen according to literature data and applied in the LIDAR retrieval, are reasonable and span across the LR estimated from the in-situ measurements. However, it is important to note that these in-situ derived LRs solely serve as plausibility check and were not used for any further calculations or retrievals.

Added text: Abstract: line 13:

Note, however, that the comparison was for the most part done in the altitude range where the overlap function is incomplete and accordingly uncertainties are larger.

Revised text: Conclusion: line 17:

The temporal variability of aerosol particle optical properties due to the development of the PBL is most pronounced at altitudes below 1000 m above ground. This is a very challenging range for remote sensing techniques as the incomplete overlap of the laser beam with the field of view results in increased uncertainty.

Some other issues, refers to the need of explicit and detailed information on uncertainties I requested in my previous review (General comment 2). The treatment of uncertainties must be extensive to the different sections of the manuscript, those dealing with in-situ and those dealing with remote sensing. In my previous review I asked the authors to comment on the uncertainties in the retrieval of PBL from the ceilometer. There is an extended literature on this issue and the authors must indicate the difficulty in retrieving the PBL height from ceilometer when there is a residual layer on top of the PBL.

First, we would like to note that we did not use an automated algorithm to retrieve the mixing layer height (MLH). In order to explain exactly how we retrieved it we adapted the text of the manuscript as stated below.

It is well known that the MLH is an information retrieved rather than measured. That is because the definition of MLH suffers from a number of uncertainties, and most methods based either on radio sounding products (Ri number, T or RH gradients, etc.) or remote-sensing data (e.g. sound/sonic detecting and ranging systems - SODAR, radio acoustic sounding system - RASS, LIDAR) often result in quite different estimates of the MLH (e.g. Seibert et al., 2000, Haeffelin et al, 2012). In this respect, boundary layer meteorologists know a "true" measurement (to be also used for validation) of MLH to be quite a “volatile” task. Seibert et al., (2000) indicate strengths and weaknesses of various methods employed to retrieve the MLH. Remote-sensing retrievals of the MLH, as done by means of Sodars, RASS, and LIDAR’s, represent the only methodologies capable of providing a continuous record of the MLH. Lidar-based retrievals exploit aerosols as tracers of the MLH. Haeffelin et al. (2012) described some best practices for the automatic retrieval of the MLH from the ceilometer signal. Di Giuseppe et al. (2011) demonstrated that automated retrievals can be reliable when an advanced (in that case Bayesian) signal analysis is performed.

Amongst other benefits, our approach avoids the "*difficulty in retrieving the PBL height from ceilometer when there is a residual layer on top of the PBL*" encountered by automatic MLH retrievals.

Seibert, P, Beyrich, F., Gryning, S. E., Joffre, S., Rasmussen, A. and Tercier, P. Review and intercomparison of operational methods for the determination of the mixing height. Atmos. Environ. 34, 1001–1027, 2000.

Added text: Section 2.1.: Page 4: line: 23-25:

The station is equipped with instruments comparable to those employed on the Zeppelin NT airship with addition of a nephelometer for a direct measurement of the aerosol scattering coefficient and a LIDAR.

In order to get an estimate of the mixing layer height at a certain time an automated LIDAR-ceilometer (Jenoptik CHM15K "Nimbus") was operated at SPC. In the present analysis we employed an operator-driven approach which avoids the major drawbacks of automated mixing layer height (MLH) retrievals (e.g. Heaffelin et al., 2012, Di Giuseppe et al., 2011). This is performed by manually evaluating the MLH by a skilled operator's visual analysis of three plots obtained by the pre-processing of the ceilometer signal (the plots are presented in the supplement): 1) the range corrected signal plot; 2) the signal's gradients plot, and 3) the signal's variance plot (e.g. Angelini et al., 2009). By observing these three plots, our trained operator manually marks on the plots a number of points (at least one per hour) matching the requirements of showing maximum signal gradients, maximum signal variance, continuity between sunrise until sunset and separation from the residual layer's gradient maxima. A spline curve is then fitted to these points to provide a continuous MLH along the day. Naturally, the MLH is not retrieved when it descends below the minimum height observed by the ceilometer (about 200 m above ground). We found, if the ML aerosol imprint is present in the signal (as it is in the ceilometer record addressed in this paper), the indetermination in the MLH retrieval to be of the order of 2-3 signal bins (i.e. ±30-45 m). Additionally, we compared the ceilometer retrieval to the MLH found from analyzing T and RH gradients from a collocated radio sounding performed at 11 UTC (the corresponding figure can be found in the supplement). Note, that the radio sounding was carried out only once every 12 hours, while ceilometer retrievals of MLH have a time resolution of minutes. The 11 UTC MLH retrieved from the radio sounding yielded a value of 753 m, while an altitude of 772 m was found from the ceilometer data at this time of day. The two retrievals agree within the ±45 m we commonly use as indetermination of our MLH retrievals. Detailed height profiles of the potential temperature (Θ), which support the findings of the ceilometer, can be found in the supplement.

Revised text: Section 3: Page 4: line: 21-26:

Results for the estimated mixing layer height are shown as the violet thick line. The typical imprecision due to the operator's choice amounts to 3 pixels, i.e. ±45m.

In order to further investigate the layering of the atmosphere we added the following three figures to the supplementary material. They illustrate height profiles of the potential temperature (Θ) and radio sounding results.

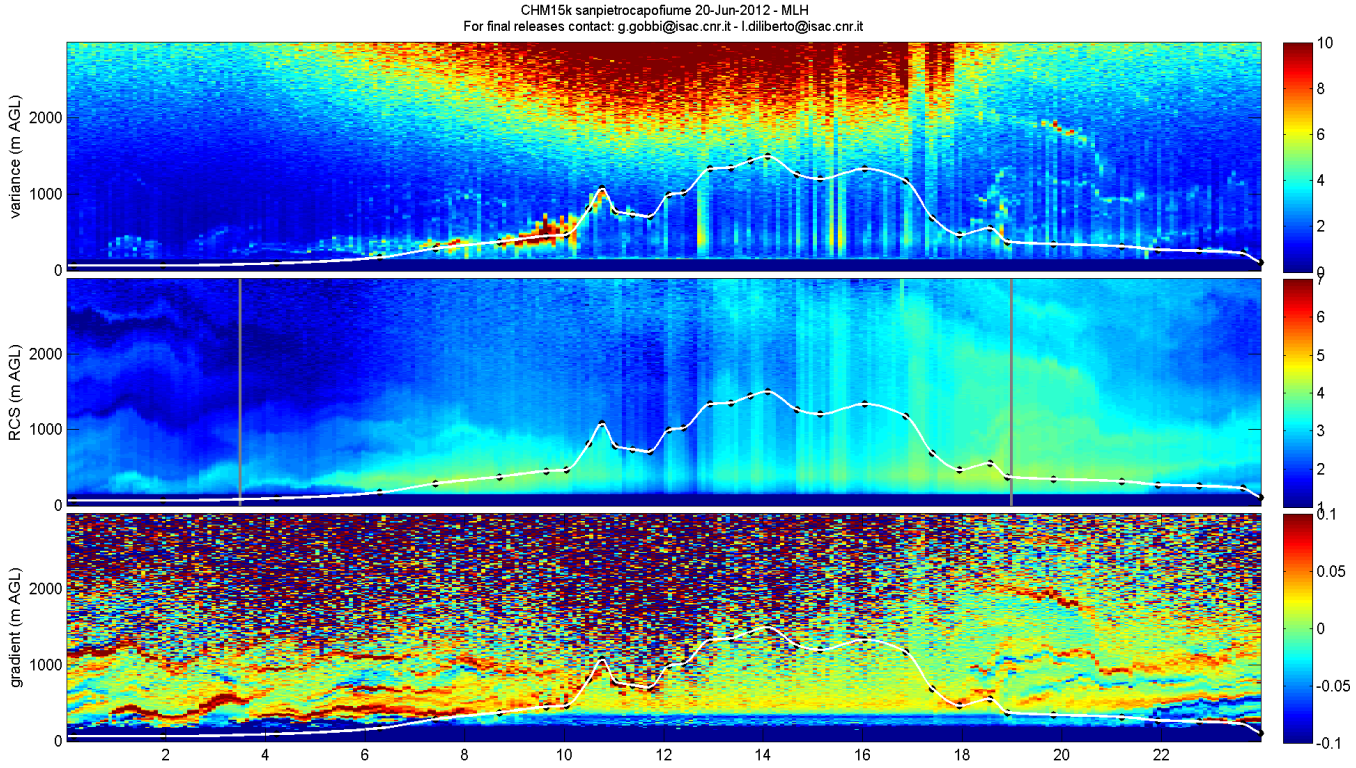

Figure: Three plots obtained by the pre-processing of the ceilometer signal. The white line represents the spline fit to the black dots marked by the operator while considering all the information from the three plots. The first panel illustrates the signal's variance plot (e.g. Angelini et al., 2009), the second the range corrected signal (RCS) plot and the third the signal's gradients plot.

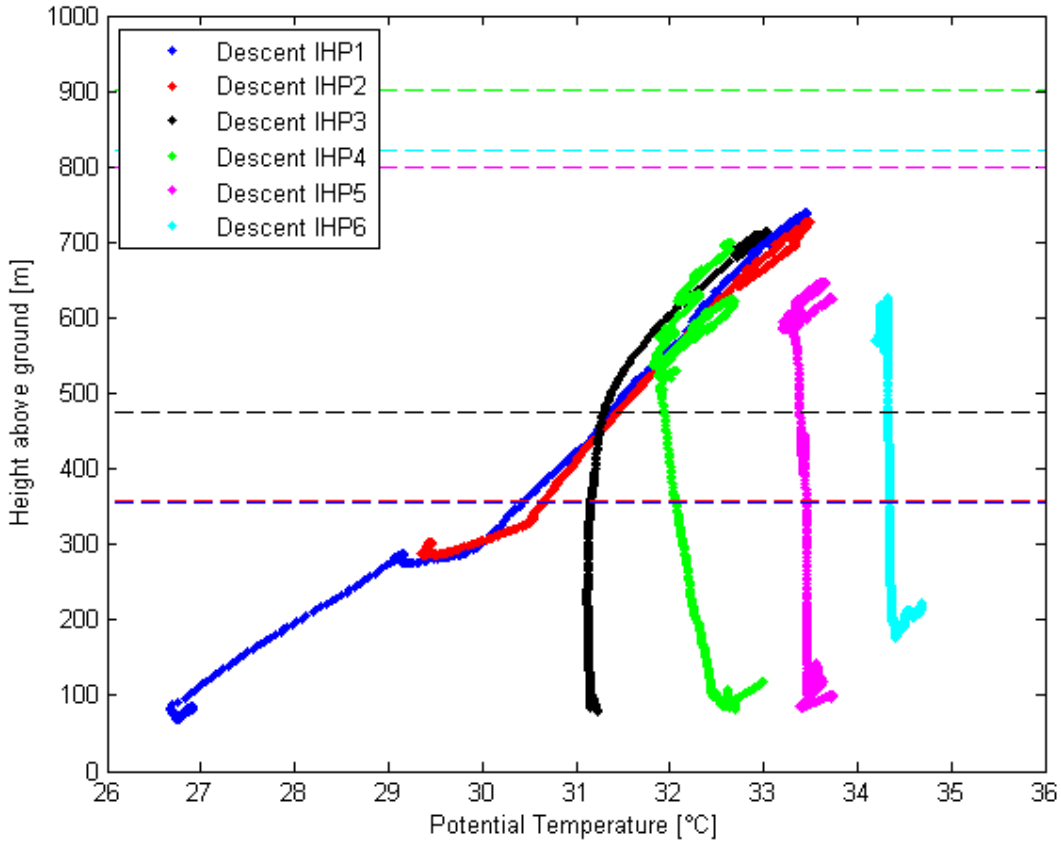

Figure: Height profiles of the potential temperature (Θ) measured aboard the Zeppelin NT during the flight on 20 June 2012. Each color represents the descents of height profiles 1-6 (IHP1-6), respectively. The horizontal lines depict the estimated mixed layer height (MLH) from the ceilometer retrieval during the six height profiles. A clear vertical structure of Θ is visible for the first two profiles, while the last four show very little or no altitude dependence at all. This indicates that the sub-layers in the PBL where still separated at the beginning of the flight and that a fully mixed layer was probed at the end. The estimated MLH retrieved from the ceilometer shows comparable results with a low MLH of approximately 350 m above ground in the morning that evolves to over 800 m above ground later during the day.

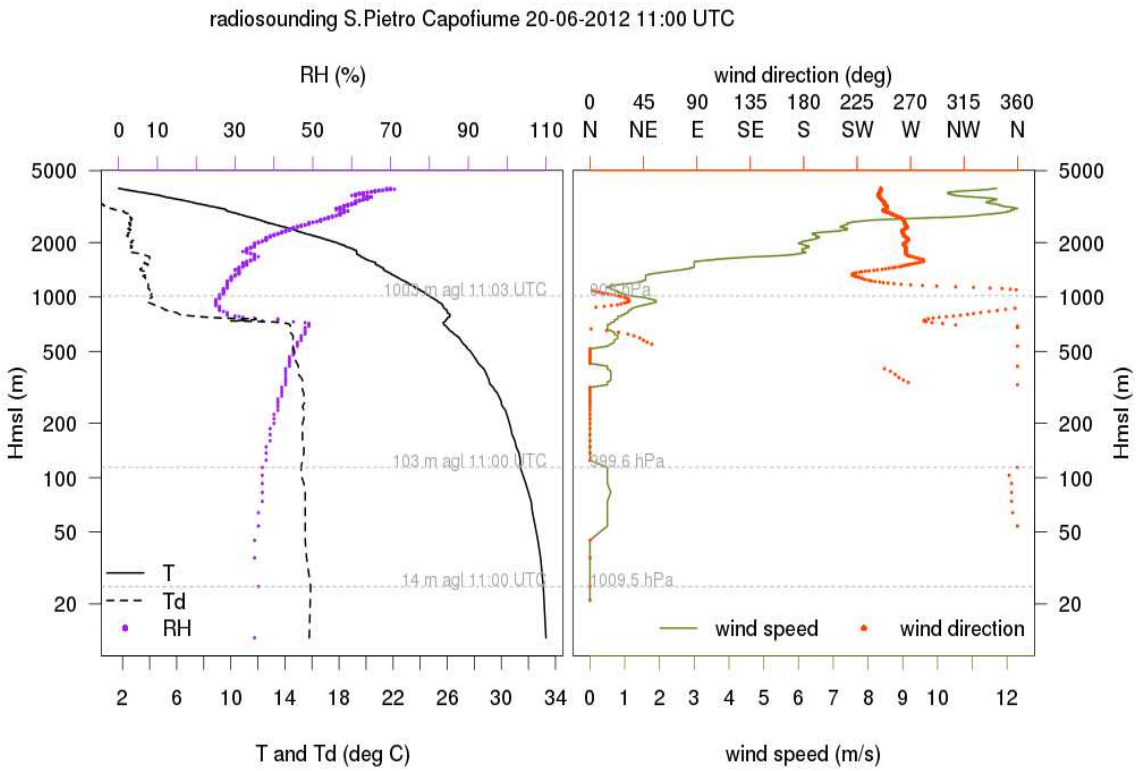

Figure: Radio sounding at San Pietro Capofiume at 11 UTC. The left panel illustrates the temperature T, dew point Td, and relative humidity RH as functions of altitude. The right panel shows wind speed and wind direction. The radio sounding yielded a MLH of 753 m.

Manuscript prepared for Atmos. Chem. Phys. Discuss.
with version 2014/09/16 7.15 Copernicus papers of the LaTeX class copernicus.cls.
Date: 18 March 2016

~~Comparison of~~ Studying the vertical aerosol extinction ~~coefficients as retrieved from~~ coefficient by comparing in-situ ~~measurements~~ airborne data and elastic back-scatter LIDAR

B. Rosati[1], E. Herrmann[1], S. Bucci[2], F. Fierli[2], F. Cairo[2], M. Gysel[1], R. Tillmann[3], J. Größ[4], G. P. Gobbi[2], L. Di Liberto[2], G. Di Donfrancesco[5], A. Wiedensohler[4], E. Weingartner[1,a], A. Virtanen[6], T. F. Mentel[3], and U. Baltensperger[1]

[1]Laboratory of Atmospheric Chemistry, Paul Scherrer Institute, 5232 Villigen PSI, Switzerland
[2]Institute of Atmospheric Sciences and Climate (ISAC-CNR), National Research Council, 00133 Rome, Italy
[3]Institute for Energy and Climate Research (IEK-8), Forschungszentrum Jülich, 52428 Jülich, Germany
[4]Leibniz Institute for Tropospheric Research, 04318 Leipzig, Germany
[5]Italian National Agency for New Technologies, Energy and Environment (ENEA), 00044 Frascati, Italy
[6]Department of Applied Physics, University of Eastern Finland, 70211 Kuopio, Finland
[a]now at: Institute for Aerosol and Sensor Technology, University of Applied Science Northwestern Switzerland, 5210 Windisch, Switzerland

Correspondence to: E. Herrmann (erik.herrmann@psi.ch)

Abstract

Vertical profiles of aerosol particle optical properties were explored in a case study near the San Pietro Capofiume (SPC) ground station during the PEGASOS Po Valley campaign in the summer of 2012. A Zeppelin NT airship was employed to investigate the effect of the dynamics of the planetary boundary layer at altitudes between $\sim$ 50–800 m above ground. Determined properties included the aerosol particle size distribution, the hygroscopic growth factor, the effective index of refraction and the light absorption coefficient. The first three parameters were used to retrieve the light scattering coefficient. Simultaneously, direct measurements of both the scattering and absorption coefficient were carried out at the SPC ground station. Additionally, a single wavelength polarization diversity elastic LIDAR system provided estimates of aerosol extinction coefficients using the Klett method to accomplish the inversion of the signal, for a vertically resolved comparison between in-situ and remote sensing results. Note, however, that the comparison was for the most part done in the altitude range where the overlap function is incomplete and accordingly uncertainties are larger. First, the airborne results at low altitudes were validated with the ground measurements. Agreement within approximately $\pm$ 25 and $\pm$ 20 % was found for the dry scattering and absorption coefficient, respectively. The single scattering albedo, ranged between 0.83 to 0.95, indicating the importance of the absorbing particles in the Po Valley region. A clear layering of the atmosphere was observed during the beginning of the flight (until $\sim$ 10:00 local time) before the mixed layer (ML) was fully developed. Highest extinction coefficients were found at low altitudes, in the new ML, while values in the residual layer, which could be probed at the beginning of the flight at elevated altitudes, were lower. At the end of the flight (after $\sim$ 12:00 local time) the ML was fully developed, resulting in constant extinction coefficients at all altitudes measured on the Zeppelin NT. LIDAR estimates captured these dynamic features well and good agreement was found for the extinction coefficients compared to the in-situ results, using fixed LIDAR ratios (LR) between 30 and 70 sr for the altitudes probed with the Zeppelin. These LR are consistent with values for continental aerosol particles that can be expected in this region.

1 Introduction

Atmospheric aerosol particles are known to interact directly with the incident solar radiation by either scattering or absorbing light. By doing so they ~~can~~ influence the Earth's radiative budget and therefore have an impact on climate (~~e.g.~~ IPCC, 2013). Due to the layering of the atmosphere, a strong vertical gradient of particle concentration is found between the Earth's surface and the lowest kilometer of the troposphere. Most emissions are trapped in this so-called planetary boundary layer (PBL) which is part of the troposphere and the layer closest to the ground. The PBL is dynamic and strongly influenced by the solar radiation (Stull, 1988). One major point of interest is to know whether surface based measurements can be used to infer aerosol radiative properties at elevated altitudes. For this purpose, remote sensing techniques ~~, like~~ such as light detection and ranging (LIDAR) instruments ~~,~~ are useful to monitor optical properties such as aerosol extinction and back-scattering coefficient over a large range of altitudes. This technique involves a pulsed laser beam to measure the back-scatter by gases and aerosol particles in the atmosphere (Klett, 1981). However, certain limitations exist for this method. One refers to the fact that accurate profiles can only be recorded above a certain threshold given by the altitude where the laser beam is completely within the field of view of the telescope (Sassen and Dodd, 1982). Below this altitude, additional assumptions have to be made in order to retrieve the optical properties and different correction schemes have been proposed (see e.g. Biavati et al., 2011). In-situ measurements on aircrafts have been used to validate remote sensing data. However, these are often limited to low RH measurements, while RH typically varies with altitude. Changes in RH may lead to changes in size, shape and index of refraction if the particles are hygroscopic and take up water; hence the optical properties would be altered. Only few studies performed RH-dependent measurements at elevated altitudes (Morgan et al., 2010; Sheridan et al., 2012) and even fewer compared these to optical measurements from LIDARs (Zieger et al., 2011; Sheridan et al., 2012). Additionally, measurements on aircrafts commonly focus on altitudes of several km above ground therefore usually starting at the upper part or even above the PBL. Due to the limited number of measurements focusing

on changes in the PBL over the course of the day, the effects of PBL dynamics on aerosol properties remain poorly understood.

During the PEGASOS (Pan-European Gas–AeroSOls-climate interaction Study) project a Zeppelin NT airship was employed to study aerosols at altitudes between 50–800 m above ground. This offered a unique opportunity to compare in-situ measurements to low altitude LIDAR estimates, which is known to be challenging (see e.g. Sheridan et al., 2012). Data from a flight on 20 June 2012 in the Po Valley (Italy) will be used. Rosati et al. (2015b) presented results of hygroscopicity measurements combined with chemical composition data for the vertical profiles on the same day. Here, this same data is used to calculate in-situ extinction coefficients and compare them to LIDAR observations. A consistency check for the airborne results is done by comparison to ground based data.

2 Experimental

2.1 Site and flight description

During the PEGASOS measurement campaign 2012, vertical profiles were performed near the San Pietro Capofiume (SPC) ground station located in the Po Valley in Italy (see Fig. 1). The general set-up of the Zeppelin NT platform for aerosol measurements as well as meteorological data for the flight on 20 June 2012 were presented in Rosati et al. (2015b). The SPC station is ~~suited to investigate air masses at a rural background area~~a rural background site well suited to investigate aerosols which have been transported over longer distances. Due to its vicinity to cities like Bologna ($\sim$ 40 km to the south-west), it also offers the possibility to study pollution from regional sources~~or aerosols transported over longer distances~~. Several campaigns have already taken place at this site focusing on variations in chemical composition as well as hygroscopic and optical properties (e.g. Mazzola et al., 2010; Saarikoski et al., 2012; Bialek et al., 2014; Decesari et al., 2014). The station is equipped with instruments comparable to those employed on the Zeppelin NT airship with

the addition of a nephelometer for a direct measurement of the aerosol scattering coefficient and a LIDAR.

In order to get an estimate of the mixing layer height at a certain time an automated LIDAR-ceilometer (Jenoptik CHM15K "Nimbus") was operated at SPC. In the present analysis we employed an operator-driven approach which avoids the major drawbacks of automated mixing layer height (MLH) retrievals (e.g. Angelini et al., 2009; Haeffelin et al., 2012; Di Giuseppe et al., 2012). This is performed by manually evaluating the MLH by a skilled operator's visual analysis of three plots obtained by the pre-processing of the ceilometer signal (the plots are presented in the supplement): 1) the range corrected signal plot; 2) the signal's gradients plot, and 3) the signal's variance plot (e.g. Angelini et al., 2009). By observing these three plots, the trained operator manually marks a number of points on the plots (at least one per hour) matching the requirements of showing maximum signal gradients, maximum signal variance, continuity between sunrise until sunset and separation from the residual layer's gradient maxima. A spline curve is then fitted to these points to provide a continuous MLH over time. Naturally, the MLH is not retrieved when it descends below the minimum height observed by the ceilometer (about 200 m above ground). We found, if the ML aerosol imprint is present in the signal (as it is in the ceilometer record addressed in this paper), the indetermination in the MLH retrieval is of the order of 2-3 signal bins (i.e. $\pm$30-45 m). Additionally, we compared the ceilometer retrieval to the MLH found by analyzing T and RH gradients from a collocated radio sounding performed at 11 UTC (the corresponding figure can be found in the supplement). Note, that the radio sounding was carried out only once every 12 hours, while ceilometer retrievals of MLH have a time resolution of minutes. The 11 UTC MLH retrieved from the radio sounding yielded a value of 753 m, while an altitude of 772 m was found from the ceilometer data at this time of day. The two retrievals agree within the $\pm$45 m we commonly use as uncertainty of our MLH retrievals. Detailed height profiles of the potential temperature (Θ), which support the findings of the ceilometer, can be found in the supplement.

On 20 June 2012 a set of vertical profiles of aerosol particle ~~optical~~ properties were obtained between 50–800 m near the SPC ground station starting from the early morning (∼ 08:00 local time (LT)) and ending in the early afternoon (∼ 14:00 LT) with a short refuel break in between (∼ 10:00–11:00 LT). The goal of these flights was to study how the dynamics of the PBL affects the vertical ~~distribution and~~ and temporal variability of the ~~aerosol properties~~observed and derived aerosol parameters. The day was characterized by low wind speeds of approximately 2–3 $m\,s^{-1}$ with mainly westerly wind direction. Therefore, local emissions are expected to have a strong influence.

2.2 Instrumentation

In the following we present only those of all PEGASOS instruments used for this analysis.

2.2.1 Aerosol particle size distributions

To obtain dry aerosol particle size distributions, scanning mobility particle sizers (SMPS; e.g. Wiedensohler et al., 2012) and a white-light aerosol spectrometer (WELAS; Palas GmbH, Type 2300; see Heim et al., 2008 or Rosati et al., 2015a for more details) were used. The WELAS is an optical instrument that uses a white-light source (OSRAM XBO-75 xenon short arc lamp) which minimizes Mie oscillations for the light scattering and enables mostly unambiguous attribution of particle optical ~~diameter~~ diameters to measured scattering cross ~~section~~ sections for most aerosol types. Nominally, the instrument covers the size range between approximately 200~~and 1050~~ nm and 10 µm but its actual range is dependent on the index of refraction of the measured particles (see below).

At the SPC ground station, an SMPS (custom-built instrument from TROPOS, Leipzig with a butanol – condensation particle counter) was used to measure the aerosol particle size distributions for dry particles with diameters between 10 and 800 nm. The SMPS system was set up in the usual way that particles were first neutralized in a bipolar particle charger, then classified according to their electrical mobility in a differential mobility analyzer (DMA) and finally counted in a condensation particle counter (CPC). The size distributions

were corrected for multiply charged particles. The airborne data sets were recorded using an SMPS (TSI Inc., DMA Model 3081 and water – CPC Model 3786) and a WELAS resulting in a combined dry aerosol particle size distribution between about 10 nm and 10 µm. The airborne SMPS only measured particle sizes between 10–430 nm. The WELAS system recorded particle sizes above approximately 500 nm, since observations for smaller particles were discarded, as they were potentially biased by a reduced counting efficiency (Rosati et al., 2015a). The size range of airborne SMPS and WELAS thus did not overlap; therefore a spline interpolation was performed in between using the surface area size distributions measured by the instruments. The combination of data from both measurements made it possible to cover the full optically relevant size range. The resulting size distributions were estimated to have an uncertainty of ± 12 and ± 5 % for the number concentrations and the diameters, respectively.

2.2.2 Hygroscopic properties

The airborne platform was equipped with the white-light humidified optical particle spectrometer (WHOPS) to measure the hygroscopic growth factor (GF), defined as the ratio of the particle diameter at an elevated RH (D_{wet}) to the one at dry conditions (D_{dry}):

$$\text{GF(RH)} = \frac{D_{\text{wet}}(\text{RH})}{D_{\text{dry}}} \tag{1}$$

The GF was recorded for dry particle diameters of 500 nm. A detailed description of the design and specifications of the WHOPS and associated data analysis procedures was provided in Rosati et al. (2015a). Briefly, particles are first dried before quasi-monodisperse aerosol particles with a well-defined dry diameter (D_{dry}) are selected in a DMA. The scattering cross section ("optical size") of these particles is then alternately determined at dry conditions and at high RH by either leading the particles directly into the WELAS or by first exposing them to typically 95 % RH before measurement in the WELAS. The dry responses from the two different techniques can then be compared to infer the index of refraction of the selected dry particles (details on the approach are presented in Rosati et al., 2015a).

Assuming an index of refraction, the scattering cross section can be calculated from the dry diameter using Mie theory. The index of refraction that brings this theoretical scattering cross section into agreement with the measured one, is defined as the effective index of refraction in the context of this work. The term "effective" reflects the fact that several simplifying assumptions are made in the Mie calculations. The particles are assumed to be perfectly spherical and present a homogeneous internal mixture, and the imaginary part of the index of refraction is assumed to be zero. The latter approximation is justified by the fact that scattering coefficients exceed absorption coefficients by a factor of 8 (see Sect. 2.2.2 and Fig. 4). In this manner, an average effective index of refraction of 1.43 ± 0.04 ($\pm$ 1σ uncertainty) was determined by Rosati et al. (2015b) for the particles probed during the flight in this study. The humidified mode aims at measuring the hygroscopic growth factors of the selected particles, following the approach in Rosati et al. (2015a). For this purpose, the measured scattering cross section of the humidified particles is converted to an optical diameter representing D_{wet}, such that the hygroscopic growth factor can be inferred with Eq. (1). In order to obtain meaningful D_{wet} and GF values, it is crucial to use the true index of refraction of the solution droplets in the Mie calculations. The index of refraction is obtained as the volume weighted mean of the indices of refraction of the dry particles and pure water ($m_{\text{H}_2\text{O}} = 1.333$) according to the respective volume fractions at a certain GF. The relative uncertainty of the inferred hygroscopic growth factors was found to be approximately $\pm 10\,\%$ for GF < 3 (Rosati et al., 2015a).

The ground station in SPC was equipped with a hygroscopicity tandem differential mobility analyzer (HTDMA; see e.g. Swietlicki et al., 2008). Here, GF for dry diameters of 200 nm were used (compare Rosati et al., 2015b). In the HTDMA two DMAs are operated in series and connected to a CPC. In the first DMA dry monodisperse aerosol particles are selected and then exposed to a defined elevated RH. The second DMA coupled to the CPC is used to measure the size distribution of the grown particles. The uncertainty for these HTDMA-GFs is expected to be approximately $\pm 5\,\%$, if a $\pm 2\,\%$ uncertainty is assumed for the RH measurement.

The hygroscopic growth measured with the WHOPS and the HTDMA were used to convert scattering coefficients obtained from measurements of the dry aerosol to the corresponding value at ambient RH, as detailed in Sect. 2.2.3.

2.2.3 Aerosol scattering coefficient

At the SPC ground station the total light scattering coefficients were measured with an integrating nephelometer (TSI Inc., Model 3563) at three different wavelengths of $\lambda = 635, 525$ and 450 nm behind a PM_{10} inlet system and after drying to RH $< 40\,\%$. The truncation error correction introduced by Anderson et al. (1996) was applied. The uncertainty for these measurements is estimated to be $\pm 5\,\%$. As no direct measurement of the aerosol scattering coefficient was available aboard the Zeppelin NT airship, it was inferred using the particle size distributions, the effective index of refraction and Mie theory assuming spherical particles (Mie, 1908; Bohren and Huffman, 2007). First, scattering cross sections (σ_s) as a function of particle diameter (D) were calculated using the wavelength of $\lambda = 520\,\text{nm}$ and the range of indices of refraction (m) measured during the flight. This specific wavelength was chosen to compare the airborne data ~~with~~ to results from the ground based and remote sensing measurements. The WHOPS retrieval yielded on average $m = 1.43 \pm 0.04$, while a comparison to the directly measured scattering coefficients from SPC showed that using $m = 1.43 \pm 0.02$ for the Mie calculations is enough to explain the variability of the nephelometer data. Second, the scattering coefficients (μ_s) were obtained by integrating the product of σ_s and the measured number size distributions $\left(\frac{\mathrm{d}N}{\mathrm{d}D}\right)$ over the full diameter range:

$$\mu_{s,j}(\lambda, m, D) = \int_{D_{min}}^{D_{max}} \sigma_s(\lambda, m_j, D_j) \cdot \frac{\mathrm{d}N}{\mathrm{d}D_j} \mathrm{d}D_j \tag{2}$$

The index j can be replaced by dry when calculating the dry scattering coefficients or by wet when the humidified coefficient is regarded. An uncertainty analysis showed that changes in the index of refraction caused the biggest errors in $\mu_{s,dry}$. Together with the

size distribution uncertainty an overall uncertainty of approximately $\pm 18\,\%$ was obtained for the dry scattering coefficient. It is possible to directly compare ground based and airborne measurements with each other, as both were performed at dry conditions.

For comparison with the LIDAR remote sensing data, the Zeppelin measurements were corrected to ambient RH. The importance of this correction was previously studied by using a humidified nephelometer (Wet-Neph; Fierz-Schmidhauser et al., 2010a, b; Zieger et al., 2010, 2011, 2012, 2013). This instrument directly measures the scattering enhancement due to elevated RH, which can be described by a wavelength (λ) dependent scattering enhancement factor $f(\mathrm{RH}, \lambda)$:

$$f(\mathrm{RH}, \lambda) = \frac{\mu_{\mathrm{s,wet}}(\mathrm{RH}, \lambda)}{\mu_{\mathrm{s,dry}}(\lambda)} \tag{3}$$

As no such instrument was available during the PEGASOS campaign, the humidity correction was achieved by combining the GF results at 95 % RH from Rosati et al. (2015b) with the ambient RH measurements to determine an ambient light scattering coefficient. This makes it possible to infer the effect of ~~the~~ hygroscopic growth on the light scattering coefficient ~~through considering the~~ by considering its effect on the size distribution. The GF was measured for monodisperse aerosol particles of 500 nm but we assume it to be constant over the full size range. Small particles ($D < 200\,\mathrm{nm}$) could potentially have a different hygroscopic behavior since species like sea salt or mineral dust are predominately found in the larger size ranges. Nevertheless, this assumption is deemed satisfactory since small particles have a minor ~~contribution~~ impact on light scattering compared to the effect of the larger sizes. In order to obtain an ambient GF (GF for $\mathrm{RH_{ambient}}$) the results at $\mathrm{RH} = 95\,\%$ were recalculated for $\mathrm{RH_{ambient}}$ using the semi-empirical κ-Köhler theory introduced by Petters and Kreidenweis (2007):

$$\kappa = \frac{(\mathrm{GF(RH)}^3 - 1) \cdot (1 - a_{\mathrm{w}})}{a_{\mathrm{w}}} \tag{4}$$

where a_w is the water activity which can be inferred from the RH and equilibrium droplet diameter (D_{wet}):

$$a_w = \frac{RH}{\exp\left(\frac{4\sigma_{s/a}M_w}{RT\rho_w D_{wet}}\right)} \quad (5)$$

Here, $\sigma_{s/a}$ is the surface tension of the solution/air interface, M_w the molecular mass of water, R the ideal gas constant, T the absolute temperature and ρ_w the density of water. We assume κ to be the same at all RH although this might introduce some bias as former studies found changes of κ with RH at elevated organic fractions (e.g. Pajunoja et al., 2015). However, the potential deviation due to this simplification is small in our case since the GF is anyways small at the moderate RH encountered in this study.

The recalculated GF for $RH_{ambient}$ were further used to retrieve humidified aerosol particle size distributions from the measured dry size distributions. The water uptake has also an influence on the index of refraction which is taken into account for the Mie calculations by applying a volume weighting mixing rule to determine the index of refraction of the grown particles. Finally a humid scattering coefficient ($\mu_{s,wet}$) was calculated according to Eq. (2). By propagating the uncertainties of the single parameters in Eq. (2), a mean uncertainty of approximately ±18 % was found for $\mu_{s,wet}$. The ratio of $\mu_{s,wet}$ to $\mu_{s,dry}$ was finally used to calculate $f(RH)$ according to Eq. (3). The uncertainty in $f(RH)$ amounted on average to ±25 %. Also the ground based data set was corrected for changes due to elevated RH by using hygroscopicity results from the HTDMA (see Sect. 2.2.2 for more details). In this case the size distributions from the SPC-SMPS were recalculated including adjustments for the $RH_{ambient}$ in SPC. Then the $f(RH)$ was obtained with Eq. (3) using the dry and humidified size distributions measured and retrieved in SPC and finally it was applied ~~on~~ to the directly measured scattering coefficients obtained from the nephelometer to get $\mu_{s,wet}$. The uncertainty in $f(RH)$-SPC amounted on average to ±26 %, while approximately ±27 % are found for $\mu_{s,wet}$-SPC.

2.2.4 Aerosol absorption coefficient

A portable aethalometer (AE42, MAGEE Scientific; Berkeley, USA) was mounted in the Zeppelin NT for a continuous measurement of the aerosol light absorbing properties at seven wavelengths. This instrument monitors the attenuation of light through a quartz fiber filter. The signal was then corrected as proposed by Weingartner et al. (2003) for multiple scattering in the filter matrix ("C value") and the so called shadowing effect ("f value"). A C value of 4.75 for $\lambda = 520\,\mathrm{nm}$ was used according to personal communications with J. P. Putaud who performed a comparison between an aethalometer (model AE31) and a MAAP in summer 2012 in Ispra, Italy. The f value amounted to 1.06 on average. For the flights a maximal attenuation of 70 % and a flow rate of $4\,\mathrm{L\,min^{-1}}$ were chosen. The estimated uncertainty for this data set is $\pm 20\,\%$.

A multi-angle absorption photometer (MAAP; Thermo Scientific Carusso; Model 5012; Petzold et al., 2005) was employed at the SPC ground station. It measures the light attenuation and scattering by particles deposited on a filter. The nominal wavelength is 670 nm, however, the actual wavelength was found to be 637 nm (Müller et al., 2011). A $\pm 10\,\%$ uncertainty is estimated for these results. In order to combine these measurements with those of the scattering coefficients, the values were extrapolated to a wavelength of 520 nm using the Ångström exponent (α_a) from the multiple wavelength measurement of the aethalometer. No aethalometer was available in SPC and therefore α_a was applied as obtained from the airborne data set. To calculate α_a from the airborne data set Eq. (1b) from Moosmüller et al. (2011) was applied, choosing the adjoining wavelengths $\lambda 1$ and $\lambda 2$:

$$\alpha_\mathrm{a}(\lambda 1, \lambda 2) = -\frac{\ln(\alpha(\lambda 1)) - \ln(\alpha(\lambda 2))}{\ln(\lambda 1) - \ln(\lambda 2)} \tag{6}$$

During this flight the absorption Ångström exponent α_a amounted on average to 0.93 ± 0.15 (mean $\pm$ SD). Then Eq. (7) was applied to recalculate μ_a measured by the MAAP to the wavelength of interest (520 nm):

$$\mu_{a,MAAP}(520\,nm) = \mu_{a,MAAP}(637\,nm) \cdot \left(\frac{520\,nm}{637\,nm}\right)^{-\alpha_a} \quad (7)$$

This introduces an additional uncertainty of 3 %, leading to a final uncertainty in $\mu_{a,MAAP}(520\,nm)$ of $\pm 13\,\%$. At both locations μ_a was assumed not to vary substantially with ambient RH. This assumption is justified by several reasons: μ_a can potentially be enhanced by a shell around an absorbing particle ("lensing effect"; Bond et al., 2006), however the magnitude of this effect is not clear yet due to controversial findings (e.g. Cappa et al., 2012 for ambient aerosol). Nessler et al. (2005) presented theoretical calculations to investigate changes in the absorption coefficient due to hygroscopic growth. In order to study RH effects, they compared the dry and humidified responses and found only small enhancement of the absorption coefficients at GF similar to the ones which were found in our study. Therefore the effect is expected to be small for this case study.

2.2.5 Aerosol extinction coefficient

The extinction coefficient (μ_e) can be calculated as the sum of the absorption and scattering coefficient.

$$\mu_e(RH) = \mu_a + \mu_s(RH) \quad (8)$$

For the airborne as well as ground based measurements the dry (RH < 30–$40\,\%$ as recommended by WMO/GAW, 2003) and wet (ambient RH) extinction coefficients were retrieved. In this respect, the calculation of the airborne scattering coefficient relies on the measured particle size distribution, the retrieved index of refraction of the dry particles and their hygroscopic growth. The most crucial parameter is the selection of the index of refraction, which leads to the largest uncertainties ~~for~~ of the scattering coefficient. The absorption coefficient, on the other hand, is assumed not to vary substantially with ambient RH and therefore no ambient correction was applied. However, the ground based absorption coefficient had to be recalculated for a different wavelength using Eq. (7). In order to do so, the

Ångström exponent obtained from the airborne data-set was used. The scattering coefficient is strongly dependent on RH and was therefore corrected by measurements of the particles' hygroscopic growth (see Sect. 2.2.3).The propagated measurement uncertainties for $\mu_{e,dry}$ and $\mu_{e,wet}$ amount to ~ 6 and $\sim 24\,\%$, respectively, at the SPC ground site, while an uncertainty of approximately 18 % is found for both on the aircraft. Please note, that for the airborne data set the relatively large uncertainty in $f(\mathrm{RH})$ is not propagated into the extinction results since the directly calculated $\mu_{s,wet}$ are used for Eq. (8). The ambient ground based results, however, are influenced by this uncertainty because $f(\mathrm{RH})$ is applied on the directly measured dry scattering coefficients from SPC.

Moreover In addition to the instrumentation described so far, a single wavelength polarization diversity elastic LIDAR system was deployed at the SPC ground station. This instrument uses a 532 nm pulsed Nd-YAG laser source, with a pulse duration of 1 ns, energy of 400 µJ and a repetition rate of 1 kHz. The LIDAR system collects the radiation elastically back-scattered from the atmosphere (Rayleigh scattering) by separately detecting its parallel and cross polarization components with respect to the polarization of the laser. Additional technical details of the systems are presented in Cairo et al. (2012). The overlap of the laser beam within the field of view (FOV) of the detector begins at a few tens of meters from the system, and is complete at a few hundred meters (50 and 300 m, respectively, in the simple approximation of a conical laser beam and telescope FOV). A nitrogen Raman scattering channel at 608 nm is also present, however these data are available only for nighttime conditions. This channel, which collects a signal proportional to the atmospheric molecular density, is used for the correction of the Rayleigh signal coming from the region of partial superposition between laser and FOV, the Partial Overlap Region (POR) where the back-scattered signal is partially lost. This correction is done by comparing the Raman signal received from the POR with the molecular density profile obtained by collocated simultaneous pressure and temperature balloon measurements, and thus retrieving an overlap correction function, from the ratio of the Raman signal to the molecular density. Uncertainties in the determination of the overlap function arise mainly from the pressure and temperature uncertainties, and from the Raman signal counting statistics and are reflected

in inaccuracies in the reconstructed signal of around 10 % at 100 m, rapidly decreasing upward. The system provides a profile of back-scatter ratio (R) and Volume Depolarization Ratio (DR) every 5 min for an elevation of up to 15 km, where R and DR are defined as:

$$R = \frac{(\beta_{\mathsf{a}} + \beta_{\mathsf{m}})}{\beta_{\mathsf{m}}} \tag{9}$$

$$\mathrm{DR} = \frac{(\beta_{\mathsf{a}} + \beta_{\mathsf{m}})^{\mathsf{c}}}{(\beta_{\mathsf{a}} + \beta_{\mathsf{m}})^{\mathsf{p}}} \tag{10}$$

Herein β_{a} and β_{m} are the aerosol and molecular back-scattering coefficient, respectively, and the superscripts p and c refer to their contribution in the parallel and cross polarized back-scattering. R and DR assume the value of 1 and 1.4 % respectively, in regions supposed to be free of aerosol at a normalization altitude $z0$, usually above 7 km. This normalization procedure introduces an additional possible inaccuracy in the data produced, as the derived back-scatter and extinction coefficients at any height z below $z0$, depends not only on the signal at z, but also on the extinction between z and $z0$, on the ratio of the signal at z to the one at $z0$ and on the assumed values of R and DR at $z0$ ~~Russell et al. (1979)~~(Russell et al., 1979). For the ~~here presented data~~ data presented here, we have performed a sensitivity test by varying the normalization height $z0$ subjectively chosen in the region we supposed to be free of aerosol. This resulted in a dispersion of the extinction data at altitudes below 1000 m in the order of 15 %. Therefore, the overall uncertainty for the LIDAR profiles is estimated to be approximately 25 %. Increased values of R indicate the presence of aerosol, while departures of DR from its molecular value are indicative of depolarizing ($\mathrm{DR} > 1.4\,\%$) or not-depolarizing ($\mathrm{DR} < 1.4\,\%$) aerosol. The uncertainty associated ~~to~~ with the data from the LIDAR used in this study is extensively discussed in Cairo et al. (2012). The minimum relative uncertainty on R for a 60 s measurement is 3 %. This corresponds to a minimum detectable β_{a} of $0.05 \times 10^{-6}\,\mathrm{m^{-1}\,sr^{-1}}$, at a signal to noise ratio of 100 %. This threshold level is reached close to the upper edge of the POR, at approximately 800 m, where the back-scattered signal attains its maximum and decreases ~~upward~~ upwards because of increased distance from the LIDAR, and ~~downward~~

due to downwards due to an increased loss of signal of in the progressively incomplete overlap between the laser beam and the telescope FOV. The back-scattered Rayleigh signal, which is only partially collected from the POR, is multiplied by the overlap correction function to reconstruct its entirety over that region. This correction is accepted if the reconstructed signal exceeds the raw signal by no more than a factor of 20. This corresponds to an acceptable reconstruction from approximately 100 m upward. As already stated, this brings causes a possible inaccuracy in the order of 10 % on of the reconstructed signal. Random errors, mainly arising from poor signal statistics, add to this uncertainty and only these are reported as error bars in our plots.

The inversion of the LIDAR signal is accomplished with the Klett method (Klett, 1981) using piecewise constant extinction to back-scatter ratio (a.k.a. LIDAR ratio LR) values:

$$\mathrm{LR} = \frac{\mu_{\mathsf{e}}}{\beta_{\mathsf{a}}} \tag{11}$$

and calibrating the profile by finding an atmospheric region supposed to be free of aerosol particles, usually above 8 km. The value of LR determines the aerosol extinction coefficient, once the aerosol back-scatter, β_{a}, has been retrieved from the LIDAR measurements. The values of LR to be used in the inversion are iteratively defined during the inversion procedure itself, by inspecting at each step of the signal extinction correction, the tentative values of R and DR. In regions of different aerosol occurrence, desert dust is characterized by LR ~ 50 sr (Müller et al., 2007) and DR greater than 10 % while biomass burning aerosol commonly has a LR of around 60–70 sr and a DR often lower than 10 % (Murayama et al., 1999; Ferrare et al., 2001; Fiebig et al., 2002; Dahlkötter et al., 2014). Table 1 shows a list of LR used in our inversion, classified according to R, DR and altitude. The Po Valley aerosol is predominantly of continental origin and therefore LR values between 30 and 70 sr seem to fit best as found using the CALIPSO model by Omar et al. (2009) for clean and polluted continental aerosol particles, respectively, both at $\lambda = 532$ nm. These values agree well with model results for continental aerosol presented by Barnaba and Gobbi (2004) who found LR values of 60 sr. Measurements performed in Southern Italy found LR values of approximately 50 sr below 2 km at a wavelength of 351 nm (Pisani, 2006; De Tomasi et al., 2006).

Discrepancies in LR may arise from the selected method to retrieve it and from the exact location. For instance, Müller et al. (2007) showed that comparing elastic LIDAR against AERONET sun photometers generally yields higher LR compared to LR directly from Raman LIDARS. In order to evaluate the LR assumption from literature data, we performed Mie calculations for the back-scatter coefficients using the airborne in-situ data. By applying Eq. (11) the LR was calculated and yielded values between 51-67 sr, with a mean value of 58 ± 4 sr. These results strongly support our LR selection from the literature. However, it is important to note that these in-situ derived LRs solely serve as plausibility check and were not used for any further calculations or retrievals. We also compared aerosol optical depth (AOD) obtained from the column-integrated LIDAR extinction (at 532 nm) to the AOD from a sun sun-photometer (at 500 nm) at the same site (Campanelli et al., 2007) within the framework of the SKYrad NETwork (http://atmos2.cr.chiba-u.jp/skynet/). The comparison of the AOD variability during the time frame of the PEGASOS campaign showed good agreement between the two data sets. For this period LIDAR derived AOD, using a LR equal to 70 sr, yielded on average 7 % higher values than those from the sun photometer. A sensitivity study changing the value of LR to 50 and 30 sr resulted in underestimations of 5 and 25 %, respectively. Thus, in this range of LR values, LIDAR agrees with the sun-photometer in a column-integrated sense, within the reported limit. The Supplement provides an in-depth discussion of LIDAR data treatment.

3 Results and discussion

Figure 2 presents a basic overview of the flight on 20 June 2012: two altitudes were probed at approximately 100 and 700 m above ground. Results for the estimated mixing layer height ~~(retrieved from a Jenoptik CHM15K "Nimbus" automated LIDAR-ceilometer operated at SPC, e.g. Angelini et al., 2009; Haeffelin et al., 2012; Di Giuseppe et al., 2012)~~ are shown as the violet thick line. ~~Retrieval of the estimated mixing layer height is performed by operating on a graphical interface presenting the maximum gradient points in the signal daily plot. In this way, the operator solves the ambiguities related to multiple relative maxima~~

often present in the ceilometer signal (e.g., Angelini et al., 2009). The typical imprecision due to the operator's choice amounts to 3 pixels, i.e. ± 45 m. Additionally, Fig. 2 denotes the different layers probed inside the PBL are denoted and the profiles are labeled as $P1$ through $P6$. Rosati et al. (2015b) presented the evolution of the potential temperature and RH for this specific day, together with the estimated mixing layer height. All these quantities indicate that until $\sim$ 11:30 LT at lower altitudes the new mixed layer (ML) was measured while at $\sim$ 700 m above ground the residual layer (RL) was probed. The aerosol properties in these two layers could potentially be significantly different since the RL is mainly dependent on the PBL from the day before, while the new ML is affected by direct emissions from the same day. Then the strong increase in estimated mixing layer height points towards a fully developed ML throughout the probed altitudes after $\sim$ 12:00 LT. Aerosol particles are expected to be homogeneously distributed in this layer and therefore their properties should be comparable at all altitudes. One possible exception is the RH which may be dependent on altitude and could thus induce height dependent humidity related effects.

3.1 Aerosol particle size distributions

Figure 3 illustrates the dry surface area size distributions at different altitudes and times. This kind of distribution was chosen since the optical properties are directly dependent on the surface area of the particles. The colored lines indicate the Zeppelin NT results, where each line represents the distribution in a different layer. Since two separate instruments were combined, the contributions by each instrument as well as the region in between are marked by different symbols. At the beginning of the flight, the new ML was probed close to the ground ($\sim$ 100 m above ground) with the mode of the distribution at a diameter of $\sim$ 290 nm. In addition, during the first part of the flight, the RL was measured at $\sim$ 700 m above ground. The blue line depicts the surface area size distribution in the RL with a mode at $\sim$ 270 nm and only a small contribution by particles with diameters larger than $\sim$ 500 nm. In addition, the green and pink lines show two distributions at altitudes below 200 and above 500 m above ground, respectively, for the fully developed ML which is present after approximately 12:00 LT. The results in the fully developed ML are very similar to the ones

from the RL with the mode of the distribution at ~ 260 nm. The comparison between surface area distributions in different layers indicates that no major changes occurred throughout the flight except for a slightly larger contribution of particles above approximately 300 nm in the new ML compared to the other layers. Moreover, the surface area size distributions from the SMPS at the SPC ground station before 10:00 LT (morning; black, dashed line) and after 12:00 LT (afternoon; gray, dashed line) are shown representing the new ML and the fully developed ML, respectively. A clear shift to a smaller mode diameter is seen in the afternoon compared to the morning. Ground based and airborne results agree well, finding similar distributions for the same layers.

3.2 Vertical profiles of aerosol scattering and absorption coefficients

Dry airborne scattering coefficients were calculated using the Zeppelin size distributions illustrated in Fig. 3 and Eq. (2) and compared to the ground based scattering coefficients directly measured by the nephelometer at dry conditions. Figure 4a presents the time series of dry scattering coefficients for both, the airborne (circles) and ground based (squares) data set. Moreover, the estimated mixing layer height (gray area) is shown. Highest scattering coefficients were found early in the morning at low altitudes (in the new ML), which is seen both in the ground and Zeppelin NT data. A clear decrease was found above ~ 500 m, while flying in the RL. After approximately 12:00 LT the fully developed ML is probed and similar results are found at all altitudes, as expected.

The absorption coefficients were measured directly at both locations but by different instrumentation (aethalometer in the Zeppelin, MAAP on the ground). Figure 4b illustrates the time series of dry absorption coefficients. The squares at 0 m above ground represent the SPC data set while the circles display the airborne results. A very similar picture as for the scattering is seen with highest values early in the morning at low altitudes (new ML) and much lower values just above (RL). Also, the absorption coefficients in the new ML are well comparable at all altitudes including the ground measurements in SPC.

The temporal variations of the scattering as well as absorption coefficients can be explained as follows: the local emissions are trapped in the shallow new ML in the early morn-

ing and therefore concentrations are highest there, but there are also changes in chemical composition. The chemical composition data during this day (from aerosol mass spectrometer measurements) were presented in Rosati et al. (2015b). Maximum nitrate mass fractions around 20 % were found during the first flight hours at low altitudes on board of the Zeppelin NT airship and at the SPC ground station. Later in the day the nitrate mass fraction decreased to ~ 2 %. The enhanced nitrate fraction in the morning caused increased hygroscopicity as well as larger scattering coefficients. The low nitrate fraction found in the RL as well as the fully developed ML resulted in a decrease of the dry particle size and thus a decrease of the scattering coefficient. Once the temperature and thus the ML height increased, the aerosol concentration was diluted and nitrate evaporated, which can be seen by the decreasing scattering and absorption coefficients over time.

A quantitative comparison between the ground based and airborne measurements of the scattering and absorption coefficients is presented in Fig. 5. Only data from the lowermost flight level (below 150 m above ground) was included, as this is expected to be in the same layer as the ground station during daytime. The error bars reflect the uncertainties described in Sects. 2.2.3 and 2.2.4. The scattering coefficients (Fig. 5a) compare well most of the time except for the very early morning hours (before 09:00 LT) when discrepancies up to ~ 35 % are visible. Reasons for the differences could be local emissions, which could not be captured by both measurements due to slightly shifted locations. By using a linear fit, a regression equation of $y = 1.11 \cdot x$ was found, where y denotes the dry scattering coefficient in SPC and x the dry scattering coefficient from the Zeppelin. Figure 5b illustrates the dry absorption coefficients. In this case, the linear regression yields the equation: $y = 0.89 \cdot x$, where y represents the dry absorption coefficient in SPC and x the dry absorption coefficient from the Zeppelin. Overall, we can conclude that the airborne measurements from the lowest flight level compare well with the ground based results. Thus, the airborne data set is suitable for a comparison with the extinction coefficient profiles from the LIDAR (Sect. 3.5).

3.3 Light scattering enhancement at ambient RH

Until now only the dry aerosol particle properties were discussed, while elevated RH can alter the optical properties. Therefore, the ambient RH has to be considered in order to retrieve the scattering enhancement factors and ambient scattering coefficients. For this purpose GF measurements along with ambient RH measurements were used for the calculations described in Sect. 2.2.3. Figure 6 displays the ambient RH (blue line) present at different altitudes during the flight with the Zeppelin NT. The ambient temperature during the flight ranged between 24 and 33 °C. Clear differences with altitude were observed when flying in the fully developed ML while comparable temperatures were found in the new ML and the RL at the beginning of the flight. In addition, also the airborne GF values, recalculated for the ambient RH (see Sect. 2.2.3), are shown in Fig. 6 as well as the scattering enhancement factor $f(\mathrm{RH})$. During the first flight hours the ambient RH was highest reaching values of approximately 60 % at low altitudes, resulting in $f(\mathrm{RH})$ values up to ~ 1.7 in the new ML. These high $f(\mathrm{RH})$ values are not only a function of RH but also of the chemical composition and especially of the fraction of inorganic species present in the particles. As described already in the previous section (Sect. 3.2) an enhanced fraction of nitrates was found in the new ML, which explains the enhanced hygroscopic growth at elevated RH. At the same time but higher altitude (~ 700 m; RL), RH was below ~ 40 % with $f(\mathrm{RH})$ between 1.1 and 1.2. The RL was characterized by lower RH as well as a smaller fraction of inorganics compared to the new ML and the combination of both led to smaller $f(\mathrm{RH})$ values. The second part of the flight (after $\sim$ 11:00 LT) was dominated by a low RH in the range of 25–50 % together with a low inorganic fraction, which is reflected in low $f(\mathrm{RH})$ values of 1.1 to 1.2.

The ground data recorded in SPC ~~was~~ were also corrected for scattering enhancement effects by utilizing the GF values from the HTDMA and the size distribution measurements reported in Fig. 3 (see Sect. 2.2.3). The ambient RH in SPC varied from a maximum of ~ 50 % at the beginning of the flight to ~ 25 % at the end. The $f(\mathrm{RH})$ ranged between approximately 1.3 and 1.1 during the whole flight and were applied to correct the dry scattering coefficients.

Zieger et al. (2013) previously published values from European sites with continental and background influence. At low RH of $\approx 40\,\%$, $f(\mathrm{RH})$ values between 1 and ~ 1.2 were recorded while at $\approx 60\,\%$ $f(\mathrm{RH})$ between 1 and ~ 1.8 were found. ~~When comparing these data sets good agreementis found between the two studies~~A comparison to our findings shows good agreement.

3.4 Vertical profiles of the single scattering albedo

The magnitude of the scattering coefficient exceeded the absorption coefficient on average by a factor of 7 when considering the dry values presented in Fig. 4. If also RH effects are taken into account (presented in Sect. 3.3 and Fig. 6) the ratio for the ambient coefficients reaches values of approximately 8. The relationship of the two coefficients is relevant for the sign of net aerosol radiation interactions and it is commonly described using the single scattering albedo (SSA; ω_0):

$$\omega_0 = \frac{\mu_\mathrm{s}}{\mu_\mathrm{s} + \mu_\mathrm{a}} \tag{12}$$

Figure 7 illustrates the temporal evolution of both, the dry and ambient SSA for the airborne as well as ground data. Focusing first on the dry SSA (Fig. 7a), the airborne results at $\sim 700\,\mathrm{m}$ above ground reveal a constant SSA throughout the flight. This is in agreement with expectations, as generally similar aerosol properties were observed at this altitude in the RL (morning) and fully developed ML (afternoon) in terms of size distributions (Fig. 3), composition (Rosati et al., 2015b) and optical properties (Fig. 4). Surprisingly, the dry SSA observed in the new ML before $\sim 10{:}00\,\mathrm{LT}$ at $100\,\mathrm{m}$ above ground as well as at the ground site are similar to those in the RL above. Generally, SSA is rather expected to increase with air mass age due to the formation of non-absorbing secondary aerosol components. However, the unexpected similarity of the dry SSA in the new ML and RL above can be explained with peculiar differences in chemical composition (Sect. 3.2 and Rosati et al., 2015b): the aerosol in the new ML has a strongly increased nitrate mass fraction (non-absorbing) and also a slightly increased BC mass fraction (light absorbing), compared to

the aerosol in the RL. This has compensating effects on the SSA. After, 10:00 LT the nitrate mass fraction decreases faster than the BC mass fraction in the evolving mixing layer, likely due to temperature and dilution related partitioning effects. This results in decreased dry SSA values at the ground site and 100 m above ground. In the afternoon, when the ML is fully developed, the dry SSA become again similar at all altitudes. A small vertical gradient is seen with lower values of the SSA at 100 m above ground as well as the ground station, which are likely related to the influence of local emissions. The dry SSA values observed in the three layers probed by the Zeppelin are 0.87 ± 0.01 (mean $\pm$ 1SD), 0.89 ± 0.01 and 0.87 ± 0.02 for the new ML, the RL and the fully developed ML, respectively. In this respect, the uncertainty of the dry single scattering albedo is estimated to be ± 7 % and ± 26 % for SPC and the Zeppelin, respectively. The uncertainty of the ambient single scattering albedo is estimated to be ± 36 % and ± 26 % for SPC and the airborne data, respectively.

Figure 7b displays the ambient SSA where results from Fig. 6 are taken into account. The hygroscopic growth increases the SSA as it mostly affects the scattering coefficient. The ambient RH and thus the light scattering enhancement factor is highest in the new ML. Therefore, the largest increase of the ambient SSA compared to the dry SSA is observed at low altitude in the morning. The ambient SSA values observed in the three layers probed by the Zeppelin amount to 0.92 ± 0.01 (mean $\pm$ 1SD), 0.90 ± 0.01 and 0.88 ± 0.02 for the new ML, the RL and the fully developed ML, respectively. The comparison of the SSA at dry and ambient conditions reveals that hygroscopic growth has a significant effect on the SSA even in cases with relatively low ambient RH such as this case study. Accounting for this effect is important to obtain the correct magnitude and sign of radiative forcing aerosol radiation interactions by anthropogenic aerosols.

Our results are in good agreement with previous studies performed with sun-photometers during the summer months in Ispra, located in the northern Po Valley, which found an average ambient SSA of 0.9 (Takemura et al., 2002). On the other hand, the study by Putaud et al. (2014) (also centered in Ispra) presented a long-term analysis of SSA measured with in-situ instrumentation comparable to the one employed in our case. Their mean SSA, valid for dry conditions (< 40 %), ranged between approximately 0.80 and 0.85 for the summer

months with little variation between the years 2004–2011. These values appear smaller than those from our study for the fully developed ML when RH had only a small effect on the SSA. A possible reason for this difference might be the averaging over a whole month compared to our case study performed at one specific day but also variations due to slightly different locations.

3.5 Vertically-resolved aerosol extinction coefficients

The data set of this study makes it possible to compare vertical profiles of the extinction coefficients from ~~the LIDAR retrievals with the~~ LIDAR retrievals to in-situ measurements from the airborne platform and the ground station. As presented in Sect. 2.2.5, the in-situ extinction coefficients were calculated using the retrieved scattering and measured absorption coefficients. At the same time, vertically resolved extinction coefficients were retrieved with the remote sensing LIDAR system, which provides directly results for aerosols at ambient RH (for more detail see Sect. 2.2.5). As discussed in Sect. 2.2.5 the LIDAR applied in this study cannot directly measure the extinction coefficients, therefore a LR had to be assumed. Results were calculated for three separate fixed LR of 30, 50 and 70 sr, where the value of 50 sr is assumed to be the best-guess solution for the measurement location and the prevailing aerosol type. More discussion on the selection of the LR can be found in Sect. 2.2.5. Figure 8 presents a comparison of in-situ and remote sensing results for the extinction coefficient. While the LIDAR data represent extinction at ambient RH, the in-situ measurements are shown for both, dry conditions and recalculated for ambient RH. Each height profile performed by the Zeppelin is shown in a separate panel along with the LIDAR profiles averaged over the corresponding interval. This sequence clearly shows the effects of the evolving mixing layer on the vertical distribution of aerosol loadings. Separated aerosol layers were observed during the flight profiles $P1$ and $P2$ in the morning (Fig. 8a and b). The aerosol extinction coefficient in the new ML (< 500 m above ground), which is influenced by emissions at the ground, is distinctly higher than the results in the RL above. The aerosol loadings in the new ML decrease as the ML increases ($P3$; Fig. 8c), due to stronger dilution of emissions from the ground, while the extinction coefficient in

the RL above remains constant. The upper edge of the new ML reached the highest flight altitude of the Zeppelin during $P4$ (Fig. 8d; see also Fig. 4). After that, the ML was fully developed, such that all flight levels were within the ML. This results in rather constant extinction coefficients from ground up to 600 m above ground during $P5$ and $P6$ (Fig. 8e and f). The extinction coefficient in the fully developed ML is equal to results in the RL during the first three height profiles. This indicates that the background aerosol gives the dominant contribution to the aerosol loading in the fully developed ML.

The Zeppelin NT and ground based results also illustrate the importance of hygroscopic water uptake in the new ML probed in $P1$ and $P2$ where the highest RH values were measured (see Fig. 6). At the same time in the RL, dry and humidified airborne data were about the same due to the low RH present at this elevation. The effects of hygroscopic growth were also small within the fully developed ML in the afternoon at all altitudes, when RH values were relatively low. The increased extinction coefficients retrieved by the LIDAR at approximately 300 m above ground during $P1$ and $P2$ could indicate an aerosol layer and/or an increased RH. Unfortunately, we do not have airborne data at this altitude to support either of the two hypotheses, as the Zeppelin did not fully probe this altitude level.

When comparing the results from the in-situ and remote sensing measurements, clear similarities are found. In profiles $P1$ and $P2$, an altitude dependence is visible by both techniques, with maximum values in the new ML and lowest ones in the RL. In addition, a distinct variation in μ_e between the two flight levels just above and below 400 m above ground in $P1$ is detected by the in-situ measurements (Fig. 8a), which does not coincide with remote sensing results. This is a consequence of aerosol variation during the time difference between the two "nearby" airborne measurements. It is more clearly seen in Fig. 4a, which illustrates lower μ_s values at $\sim$ 09:00 LT ($\sim$ 390 m above ground) compared to the measurements at 09:20 LT ($\sim$ 450 m above ground). At this time period the ML height was approximately at the altitude of 400 m above ground and therefore the variations can be explained by particles measured once in the RL or the entrainment zone between new ML and RL and the second time in the new ML, even though both measurements took place at comparable altitudes. For profiles $P3$–$P6$ both techniques observed small variability of the

extinction coefficient across the full altitude range. This confirms the assumption of a homogeneously mixed PBL with similar aerosol properties throughout the ML. The extinction coefficients in the fully developed ML ($P3$–$P6$) are close to those in the RL (high altitudes in $P1$ and $P2$) and lower than those in the new ML (low altitudes in $P1$ and $P2$).

When comparing absolute extinction coefficient values of the in-situ and remote sensing results for the best-guess LR $= 50$ sr, the latter tends to overestimate μ_e at the higher elevations (> 250 m) in general, while agreement is better at lower altitudes (< 250 m). In order to investigate the role of the selected LR on the agreement between in-situ and remote sensing data, a sensitivity study on the dependence of the LIDAR results on LR was carried out. In ~~this respect~~ addition to the best-guess scenario LR $= 50$ sr, LR values of 30 (orange line) and 70 sr (dark red line) ~~in addition to the best-guess scenario~~ were used, thereby covering the potential range of LR for continental aerosol reported in the literature (see Table 1). Largest discrepancies of up to 50 % between LIDAR retrievals and in-situ measurements are found for LRs of 50 and 70 sr above 600 m above ground. Choosing LR $= 30$ sr instead results in agreement within 5–20 % for these altitudes, depending on the actual flight profile. At low altitudes (< 300 m) the opposite is seen finding agreement within 15 % between in-situ and remote sensing data for a LR of 50–70 sr. This altitude dependence of the best-fit LR may on the one hand be related to true differences in aerosol properties at different altitudes, particularly in the morning, but on the other hand potential systematic biases in the overlap correction for low altitudes may also play a role.

~~However,~~ One has to note that the uncertainty ~~in~~ of the LIDAR ratio is the single most important source of inaccuracies in elastic LIDAR retrievals. A review of issues related to the assumptions ~~on~~ of LR is presented in Kovalev and Eichinger (2004). An overestimation of LR throughout the LIDAR range leads to an excessive correction of the raw data for particle attenuation, and this causes an overestimation of the retrieved aerosol extinction coefficient, the more severe the further down from the calibration altitude (Cavalieri et al., 2011). Moreover, even if the assumptions ~~on~~ of LR are valid on average, LR is not necessarily constant over the full profile. ~~There, the retrieval may get~~ The retrieval of the back-scatter coefficient ~~approximately right~~may be approximately correct, but the extinction definitely wrong, as, at

a given altitude, the local relationship between the two is simply linear in LR. One should bear in mind that a change ~~on~~ of the assumptions on LR may have two counteracting effects on the extinction retrieval: (i) a "global" one on the back-scattering coefficient, as an increase of LR decreases the value of the back-scattering coefficient the more the further down from the normalization altitude and in proportion with the optical depth from the normalization altitude ~~downward~~downwards. It should be noted that this effect is not simply linear in LR throughout the profile and depends on the particular vertical distribution of aerosol. (ii) A "local" one, as deriving the extinction coefficient by multiplying the retrieved back-scattering coefficient by the LR obviously the extinction scales linearly with LR. Which one of these two competing effects is prevailing at a given altitude, will depend on the particular aerosol vertical distribution.

4 Conclusions

A case study of aerosol particle optical properties at different altitudes in a dynamic planetary boundary layer (PBL) was performed within the PEGASOS project in the Po Valley (Italy) in 2012 using an instrumented Zeppelin NT airship. The aim of this field experiment was to investigate the effects of PBL dynamics on aerosol layering and to combine in-situ ground and airborne data of the aerosol extinction coefficients in order to compare them to remote sensing results. Additionally, ~~also~~ changes due to the hygroscopic nature of particles were considered by monitoring the hygroscopic growth factor on board of the aircraft. The temporal variability of aerosol particle optical properties due to the development of the PBL is most pronounced at altitudes below ~~one kilometer and is therefore known to be challenging~~ 1000 m above ground. This is a very challenging range for remote sensing techniques as the incomplete overlap of the laser beam with the field of view results in increased uncertainty. In this study, we present in-situ results for vertical profiles on 20 June 2012 near the San Pietro Capofiume ground station to validate remote sensing data in particular at low altitudes. Since the scattering coefficient was not measured directly on board the Zeppelin NT, it was retrieved from size distributions and index of refraction

measurements. Validation of the indirect airborne data against direct scattering coefficient measurements at the ground station revealed agreement within approximately $\pm$ 20 %. The airborne in-situ results ~~observed~~ identified the scattering coefficient as the predominant optical property at all times and altitudes being on average a factor of 8 higher than ~~compared to~~ the absorption coefficient, and the mean single scattering albedo found for this case study was of 0.89 ± 0.02 (1SD). During the early morning hours a clear layering of the PBL was observed. Increased extinction coefficients were recorded at altitudes of approximately 100 m above ground in the new mixed layer by both, the airborne and remote sensing measurements, while lower values were found in the residual layer just above. This difference can be attributed to differences in the particle number concentration, size distribution and chemical composition between the distinct layers. Besides, both techniques suggest that during the second part of the flight (early afternoon) the PBL was fully mixed due to the fact that comparable results were found at all altitudes. On the whole, the in-situ measurements of the aerosol extinction coefficient are in good agreement with remote sensing data across the whole joint altitude range from 100 to 800 m above ground for an assumed LIDAR ratio (LR) between 30 and 70 sr, as previously found for continental aerosol particles in similar regions.

The Supplement related to this article is available online at doi:10.5194/acpd-0-1-2016-supplement.

Acknowledgements. This work was supported by the EC project PEGASOS, funded by the European Commission under the Framework Programme 7 (FP7-ENV-2010-265148). We thank all PEGASOS participants for the excellent team work during the campaigns. Additionally we thank F. Holland for the analysis and maintenance of all meteorological and GPS data on the Zeppelin. We thank M. Zanatta for support concerning the nephelometers and the associated corrections. We also thank G. Bonafé for the meteorological data provided for the ground station and M. Campanelli for the sun-photometer data. M. Gysel was supported by the ERC under grant 615922-BLACARAT and E. Herrmann by MeteoSwiss in the framework of the Global Atmosphere Watch program. The

LIDAR and ceilometer data have been acquired and made available in the framework of the project SUPERSITO of ARPA Emilia Romagna (DRG no. 428/10).

References

Anderson, T., Covert, D., Marshall, S., Laucks, M., Charlson, R., Waggoner, A., Ogren, J., Caldow, R., Holm, R., Quant, F., Sem, G., Wiedensohler, A., Ahlquist, N., and Bates, T.: Performance characteristics of a high-sensitivity, three-wavelength, total scatter/backscatter nephelometer, J. Atmos. Ocean. Tech., 13, 967–986, doi:10.1175/1520-0426(1996)013<0967:PCOAHS>2.0.CO;2, 1996.

Angelini, F., Barnaba, F., Landi, T., Caporaso, L., and Gobbi, G.: Study of atmospheric aerosols and mixing layer by LIDAR, Radiat. Prot. Dosim., 137, 275–279, doi:10.1093/rpd/ncp219, 2009.

Barnaba, F. and Gobbi, G. P.: Modeling the aerosol extinction versus backscatter relationship for lidar applications: maritime and continental conditions, J. Atmos. Ocean. Tech., 21, 428–442, doi:10.1175/1520-0426(2004)021<0428:MTAEVB>2.0.CO;2, 2004.

Bialek, J., Dall Osto, M., Vaattovaara, P., Decesari, S., Ovadnevaite, J., Laaksonen, A., and O'Dowd, C.: Hygroscopic and chemical characterisation of Po Valley aerosol, Atmos. Chem. Phys., 14, 1557–1570, doi:10.5194/acp-14-1557-2014, 2014.

Biavati, G., Donfrancesco, G. D., Cairo, F., and Feist, D. G.: Correction scheme for close-range lidar returns, Appl. Optics, 50, 5872–5882, doi:10.1364/AO.50.005872, 2011.

Bohren, C. F. and Huffman, D. R.: Absorption and Scattering of Light by Small Particles, Wiley-VCH Verlag GmbH, doi:10.1002/9783527618156, 2007.

Bond, T. C., Habib, G., and Bergstrom, R. W.: Limitations in the enhancement of visible light absorption due to mixing state, J. Geophys. Res.-Atmos., 111, D20211, doi:10.1029/2006JD007315, 2006.

Cairo, F., Di Donfrancesco, G., Di Liberto, L., and Viterbini, M.: The RAMNI airborne lidar for cloud and aerosol research, Atmos. Meas. Tech., 5, 1779–1792, doi:10.5194/amt-5-1779-2012, 2012.

Campanelli, M., Estellés, V., Tomasi, C., Nakajima, T., Malvestuto, V., and Martínez-Lozano, J. A.: Application of the SKYRAD improved Langley plot method for the in situ calibration of CIMEL Sun-sky photometers, Appl. Optics, 46, 2688–2702, doi:10.1364/AO.46.002688, 2007.

Cappa, C. D., Onasch, T. B., Massoli, P., Worsnop, D. R., Bates, T. S., Cross, E. S., Davidovits, P., Hakala, J., Hayden, K. L., Jobson, B. T., Kolesar, K. R., Lack, D. A., Lerner, B. M., Li, S.-

M., Mellon, D., Nuaaman, I., Olfert, J. S., Petäjä, T., Quinn, P. K., Song, C., Subramanian, R., Williams, E. J., and Zaveri, R. A.: Radiative absorption enhancements due to the mixing state of atmospheric black carbon, Science, 337, 1078–1081, doi:10.1126/science.1223447, 2012.

Cavalieri, O., di Donfrancesco, G., Cairo, F., Fierli, F., Snels, M., Viterbini, M., Cardillo, F., Chatenet, B., Formenti, P., Marticorena, B., and Rajot, J. L.: The AMMA MULID network for aerosol characterization in West Africa, Int. J. Remote Sens., 32, 5485–5504, doi:10.1080/01431161.2010.502156, 2011.

Dahlkötter, F., Gysel, M., Sauer, D., Minikin, A., Baumann, R., Seifert, P., Ansmann, A., Fromm, M., Voigt, C., and Weinzierl, B.: The Pagami Creek smoke plume after long-range transport to the upper troposphere over Europe – aerosol properties and black carbon mixing state, Atmos. Chem. Phys., 14, 6111–6137, doi:10.5194/acp-14-6111-2014, 2014.

De Tomasi, F., Tafuro, A. M., and Perrone, M. R.: Height and seasonal dependence of aerosol optical properties over southeast Italy, J. Geophys. Res.-Atmos., 111, D10203, doi:10.1029/2005JD006779, 2006.

Decesari, S., Allan, J., Plass-Duelmer, C., Williams, B. J., Paglione, M., Facchini, M. C., O'Dowd, C., Harrison, R. M., Gietl, J. K., Coe, H., Giulianelli, L., Gobbi, G. P., Lanconelli, C., Carbone, C., Worsnop, D., Lambe, A. T., Ahern, A. T., Moretti, F., Tagliavini, E., Elste, T., Gilge, S., Zhang, Y., and Dall'Osto, M.: Measurements of the aerosol chemical composition and mixing state in the Po Valley using multiple spectroscopic techniques, Atmos. Chem. Phys., 14, 12109–12132, doi:10.5194/acp-14-12109-2014, 2014.

Di Giuseppe, F., Riccio, A., Caporaso, L., Bonafé, G., Gobbi, G., and Angelini, F.: Automatic detection of atmospheric boundary layer height using ceilometer backscatter data assisted by a boundary layer model, Q. J. Roy. Meteor. Soc., 138, 649–663, 2012.

Ferrare, R. A., Turner, D. D., Brasseur, L. H., Feltz, W. F., Dubovik, O., and Tooman, T. P.: Raman lidar measurements of the aerosol extinction-to-backscatter ratio over the Southern Great Plains, J. Geophys. Res.-Atmos., 106, 20333–20347, doi:10.1029/2000JD000144, 2001.

Fiebig, M., Petzold, A., Wandinger, U., Wendisch, M., Kiemle, C., Stifter, A., Ebert, M., Rother, T., and Leiterer, U.: Optical closure for an aerosol column: method, accuracy, and inferable properties applied to a biomass-burning aerosol and its radiative forcing, J. Geophys. Res.-Atmos., 107, LAC 12-1–LAC 12-15, doi:10.1029/2000JD000192, 2002.

Fierz-Schmidhauser, R., Zieger, P., Gysel, M., Kammermann, L., DeCarlo, P. F., Baltensperger, U., and Weingartner, E.: Measured and predicted aerosol light scattering enhancement factors at the

high alpine site Jungfraujoch, Atmos. Chem. Phys., 10, 2319–2333, doi:10.5194/acp-10-2319-2010, 2010a.

Fierz-Schmidhauser, R., Zieger, P., Wehrle, G., Jefferson, A., Ogren, J. A., Baltensperger, U., and Weingartner, E.: Measurement of relative humidity dependent light scattering of aerosols, Atmos. Meas. Tech., 3, 39–50, doi:10.5194/amt-3-39-2010, 2010b.

Haeffelin, M., Angelini, F., Morille, Y., Martucci, G., Frey, S., Gobbi, G., Lolli, S., O'Dowd, C., Sauvage, L., Xueref-Rémy, I., Wastine, B., and Feist, D.: Evaluation of mixing-height retrievals from automatic profiling lidars and ceilometers in view of future integrated networks in Europe, Bound.-Lay. Meteorol., 143, 49–75, doi:10.1007/s10546-011-9643-z, 2012.

Heim, M., Mullins, B. J., Umhauer, H., and Kasper, G.: Performance evaluation of three optical particle counters with an efficient "multimodal" calibration method, J. Aerosol Sci., 39, 1019–1031, doi:10.1016/j.jaerosci.2008.07.006, 2008.

IPCC: The Physical Science Basis. Contribution of Working Group I to the Fifth Assessment Report of the Intergovernmental Panel on Climate Change, Cambridge University Press, Cambridge, United Kingdom and New York, NY, USA, 2013.

Klett, J. D.: Stable analytical inversion solution for processing lidar returns, Appl. Optics, 20, 211–220, doi:10.1364/AO.20.000211, 1981.

Kovalev, V. A. and Eichinger, W. E.: Backscatter-to-Extinction Ratio, in: Elastic Lidar: Theory, Practice, and Analysis Methods, Wiley &Sons, Inc., 2004.

Mazzola, M., Lanconelli, C., Lupi, A., Busetto, M., Vitale, V., and Tomasi, C.: Columnar aerosol optical properties in the Po Valley, Italy, from MFRSR data, J. Geophys. Res.-Atmos., 115, D17206, doi:10.1029/2009JD013310, 2010.

Mie, G.: Beiträge zur Optik trüber Medien, speziell kolloidaler Metallösungen, Ann. Phys., 330, 377–445, doi:10.1002/andp.19083300302, 1908.

Moosmüller, H., Chakrabarty, R. K., Ehlers, K. M., and Arnott, W. P.: Absorption Ångström coefficient, brown carbon, and aerosols: basic concepts, bulk matter, and spherical particles, Atmos. Chem. Phys., 11, 1217–1225, doi:10.5194/acp-11-1217-2011, 2011.

Morgan, W. T., Allan, J. D., Bower, K. N., Esselborn, M., Harris, B., Henzing, J. S., Highwood, E. J., Kiendler-Scharr, A., McMeeking, G. R., Mensah, A. A., Northway, M. J., Osborne, S., Williams, P. I., Krejci, R., and Coe, H.: Enhancement of the aerosol direct radiative effect by semi-volatile aerosol components: airborne measurements in North-Western Europe, Atmos. Chem. Phys., 10, 8151–8171, doi:10.5194/acp-10-8151-2010, 2010.

Müller, D., Ansmann, A., Mattis, I., Tesche, M., Wandinger, U., Althausen, D., and Pisani, G.: Aerosol-type-dependent lidar ratios observed with Raman lidar, J. Geophys. Res.-Atmos., 112, D16202, doi:10.1029/2006JD008292, 2007.

Müller, T., Henzing, J. S., de Leeuw, G., Wiedensohler, A., Alastuey, A., Angelov, H., Bizjak, M., Collaud Coen, M., Engström, J. E., Gruening, C., Hillamo, R., Hoffer, A., Imre, K., Ivanow, P., Jennings, G., Sun, J. Y., Kalivitis, N., Karlsson, H., Komppula, M., Laj, P., Li, S.-M., Lunder, C., Marinoni, A., Martins dos Santos, S., Moerman, M., Nowak, A., Ogren, J. A., Petzold, A., Pichon, J. M., Rodriquez, S., Sharma, S., Sheridan, P. J., Teinilä, K., Tuch, T., Viana, M., Virkkula, A., Weingartner, E., Wilhelm, R., and Wang, Y. Q.: Characterization and intercomparison of aerosol absorption photometers: result of two intercomparison workshops, Atmos. Meas. Tech., 4, 245–268, doi:10.5194/amt-4-245-2011, 2011.

Murayama, T., Okamoto, H., Kaneyasu, N., Kamataki, H., and Miura, K.: Application of lidar depolarization measurement in the atmospheric boundary layer: effects of dust and sea-salt particles, J. Geophys. Res.-Atmos., 104, 31781–31792, doi:10.1029/1999JD900503, 1999.

Nessler, R., Weingartner, E., and Baltensperger, U.: Effect of humidity on aerosol light absorption and its implications for extinction and the single scattering albedo illustrated for a site in the lower free troposphere, J. Aerosol Sci., 36, 958–972, doi:10.1016/j.jaerosci.2004.11.012, 2005.

Omar, A. H., Winker, D. M., Kittaka, C., Vaughan, M. A., Liu, Z., Hu, Y., Trepte, C. R., Rogers, R. R., Ferrare, R. A., Lee, K.-P., Kuehn, R. E., and Hostetler, C. A.: The CALIPSO automated aerosol classification and lidar latio selection Algorithm, J. Atmos. Ocean. Tech., 26, 1994–2014, doi:10.1175/2009JTECHA1231.1, 2009.

Pajunoja, A., Lambe, A. T., Hakala, J., Rastak, N., Cummings, M. J., Brogan, J. F., Hao, L., Paramonov, M., Hong, J., Prisle, N. L., Malila, J., Romakkaniemi, S., Lehtinen, K. E. J., Laaksonen, A., Kulmala, M., Massoli, P., Onasch, T. B., Donahue, N. M., Riipinen, I., Davidovits, P., Worsnop, D. R., Petäjä, T., and Virtanen, A.: Adsorptive uptake of water by semisolid secondary organic aerosols, Geophys. Res. Lett., 42, 3063–3068, doi:10.1002/2015GL063142, 2015.

Petters, M. D. and Kreidenweis, S. M.: A single parameter representation of hygroscopic growth and cloud condensation nucleus activity, Atmos. Chem. Phys., 7, 1961–1971, doi:10.5194/acp-7-1961-2007, 2007.

Petzold, A., Schloesser, H., Sheridan, P., Arnott, W., Ogren, J., and Virkkula, A.: Evaluation of multiangle absorption photometry for measuring aerosol light absorption, Aerosol Sci. Tech., 39, 40–51, doi:10.1080/027868290901945, 2005.

Pisani, G.: Optical characterization of tropospheric aerosols in the urban area of Naples, PhD thesis, Università degli Studi di Napoli Federico III, Naples, Italy, 2006.

Putaud, J. P., Cavalli, F., Martins dos Santos, S., and Dell'Acqua, A.: Long-term trends in aerosol optical characteristics in the Po Valley, Italy, Atmos. Chem. Phys., 14, 9129–9136, doi:10.5194/acp-14-9129-2014, 2014.

Rosati, B., Wehrle, G., Gysel, M., Zieger, P., Baltensperger, U., and Weingartner, E.: The white-light humidified optical particle spectrometer (WHOPS) – a novel airborne system to characterize aerosol hygroscopicity, Atmos. Meas. Tech., 8, 921–939, doi:10.5194/amt-8-921-2015, 2015a.

Rosati, B., Gysel, M., Rubach, F., Mentel, T. F., Goger, B., Poulain, L., Schlag, P., Miettinen, P., Pajunoja, A., Virtanen, A., Bialek, J., Klein Baltink, H., Henzing, J. S., Größ, J., Gobbi, G. P., Wiedensohler, A., Kiendler-Scharr, A., O'Dowd, C., Decesari, S., Facchini, M. C., Weingartner, E., and Baltensperger, U.: Vertical profiling of aerosol hygroscopic properties in the planetary boundary layer during the PEGASOS campaigns, Atmos. Chem. Phys. Discuss., 15, 9445–9505, doi:10.5194/acpd-15-9445-2015, 2015b.

Russell, P. B., Swissler, T. J., and McCormick, M. P.: Methodology for error analysis and simulation of lidar aerosol measurements, Appl. Optics, 18, 3783–3797, doi:10.1364/AO.18.003783, 1979.

Saarikoski, S., Carbone, S., Decesari, S., Giulianelli, L., Angelini, F., Canagaratna, M., Ng, N. L., Trimborn, A., Facchini, M. C., Fuzzi, S., Hillamo, R., and Worsnop, D.: Chemical characterization of springtime submicrometer aerosol in Po Valley, Italy, Atmos. Chem. Phys., 12, 8401–8421, doi:10.5194/acp-12-8401-2012, 2012.

Sassen, K. and Dodd, G. C.: Lidar crossover function and misalignment effects, Appl. Optics, 21, 3162–3165, doi:10.1364/AO.21.003162, 1982.

Sheridan, P. J., Andrews, E., Ogren, J. A., Tackett, J. L., and Winker, D. M.: Vertical profiles of aerosol optical properties over central Illinois and comparison with surface and satellite measurements, Atmos. Chem. Phys., 12, 11695–11721, doi:10.5194/acp-12-11695-2012, 2012.

Stull, R.: An Introduction to Boundary Layer Meteorology, Kluwer Academic Publisher, Dordrecht, the Netherlands, 1988.

Swietlicki, E., Hansson, H. C., Hämeri, K., Svenningsson, B., Massling, A., McFiggans, G., McMurry, P. H., Petäjä, T., Tunved, P., Gysel, M., Topping, D., Weingartner, E., Baltensperger, U., Rissler, J., Wiedensohler, A., and Kulmala, M.: Hygroscopic properties of submicrometer atmospheric aerosol particles measured with H-TDMA instruments in various environments – a review, Tellus B, 60, 432–469, doi:10.1111/j.1600-0889.2008.00350.x, 2008.

Takemura, T., Nakajima, T., Dubovik, O., Holben, B. N., and Kinne, S.: Single-scattering albedo and radiative forcing of various aerosol species with a global three-dimensional model, J. Climate, 15, 333–352, doi:10.1175/1520-0442(2002)015<0333:SSAARF>2.0.CO;2, 2002.

Weingartner, E., Saathoff, H., Schnaiter, M., Streit, N., Bitnar, B., and Baltensperger, U.: Absorption of light by soot particles: determination of the absorption coefficient by means of aethalometers, J. Aerosol Sci., 34, 1445–1463, doi:10.1016/S0021-8502(03)00359-8, 2003.

Wiedensohler, A., Birmili, W., Nowak, A., Sonntag, A., Weinhold, K., Merkel, M., Wehner, B., Tuch, T., Pfeifer, S., Fiebig, M., Fjäraa, A. M., Asmi, E., Sellegri, K., Depuy, R., Venzac, H., Villani, P., Laj, P., Aalto, P., Ogren, J. A., Swietlicki, E., Williams, P., Roldin, P., Quincey, P., Hüglin, C., Fierz-Schmidhauser, R., Gysel, M., Weingartner, E., Riccobono, F., Santos, S., Grüning, C., Faloon, K., Beddows, D., Harrison, R., Monahan, C., Jennings, S. G., O'Dowd, C. D., Marinoni, A., Horn, H.-G., Keck, L., Jiang, J., Scheckman, J., McMurry, P. H., Deng, Z., Zhao, C. S., Moerman, M., Henzing, B., de Leeuw, G., Löschau, G., and Bastian, S.: Mobility particle size spectrometers: harmonization of technical standards and data structure to facilitate high quality long-term observations of atmospheric particle number size distributions, Atmos. Meas. Tech., 5, 657–685, doi:10.5194/amt-5-657-2012, 2012.

WMO/GAW: Aerosol Measurment Procedures Guidelines and Recommendations, Tech. Rep. Report No. 153, World Meteorological Organization, Geneve, Switzerland, available at: ftp://ftp.wmo.int/Documents/PublicWeb/arep/gaw/gaw153.pdf (last access: 3 July 2015), 2003.

Zieger, P., Fierz-Schmidhauser, R., Gysel, M., Ström, J., Henne, S., Yttri, K. E., Baltensperger, U., and Weingartner, E.: Effects of relative humidity on aerosol light scattering in the Arctic, Atmos. Chem. Phys., 10, 3875–3890, doi:10.5194/acp-10-3875-2010, 2010.

Zieger, P., Weingartner, E., Henzing, J., Moerman, M., de Leeuw, G., Mikkilä, J., Ehn, M., Petäjä, T., Clémer, K., van Roozendael, M., Yilmaz, S., Frieß, U., Irie, H., Wagner, T., Shaiganfar, R., Beirle, S., Apituley, A., Wilson, K., and Baltensperger, U.: Comparison of ambient aerosol extinction coefficients obtained from in-situ, MAX-DOAS and LIDAR measurements at Cabauw, Atmos. Chem. Phys., 11, 2603–2624, doi:10.5194/acp-11-2603-2011, 2011.

Zieger, P., Kienast-Sjögren, E., Starace, M., von Bismarck, J., Bukowiecki, N., Baltensperger, U., Wienhold, F. G., Peter, T., Ruhtz, T., Collaud Coen, M., Vuilleumier, L., Maier, O., Emili, E., Popp, C., and Weingartner, E.: Spatial variation of aerosol optical properties around the high-alpine site Jungfraujoch (3580 m a.s.l.), Atmos. Chem. Phys., 12, 7231–7249, doi:10.5194/acp-12-7231-2012, 2012.

Zieger, P., Fierz-Schmidhauser, R., Weingartner, E., and Baltensperger, U.: Effects of relative humidity on aerosol light scattering: results from different European sites, Atmos. Chem. Phys., 13, 10609–10631, doi:10.5194/acp-13-10609-2013, 2013.

Table 1. List of LIDAR ratios (LR) selected as function of back-scatter ratio (R) and depolarization ratio (DR). For Polluted continental air masses, different values have been tentatively employed for a sensitivity study.

LR [sr]	R	DR [%]	Aerosol type
70 (30–50)	$> 1.05; < 10$	< 15	polluted continental (clean continental)
50	$> 1.05; < 10$	> 10	Saharan dust
60–70	$> 1.05; < 10$	< 15	biomass burning

Figure 1. Location of the ground station San Pietro Capofiume (SPC) in Italy (adapted from http://www.italyworldclub.com/emilia/). The region Emilia Romagna is highlighted showing the main cities in the area. In the lower left corner its position within Italy is indicated.

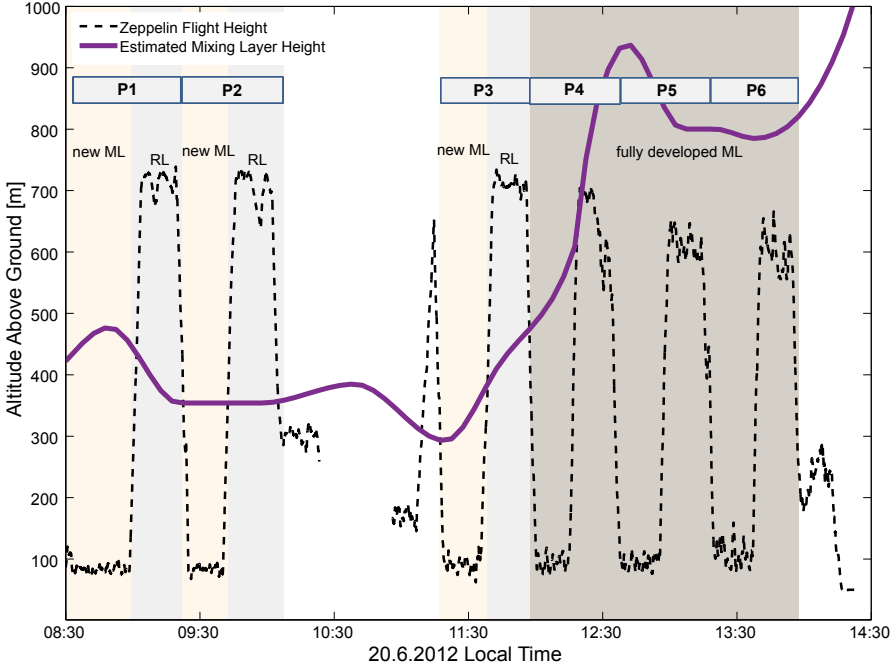

Figure 2. Overview of the flight on 20 June 2012 near San Pietro Capofiume (SPC). The black dashed line depicts the flight altitude of the Zeppelin NT airship, while the violet thick line illustrates the estimated mixing layer height. Additionally, the different layers which were probed are labeled and colored differently. Also, profiles $P1$ to $P6$ are marked.

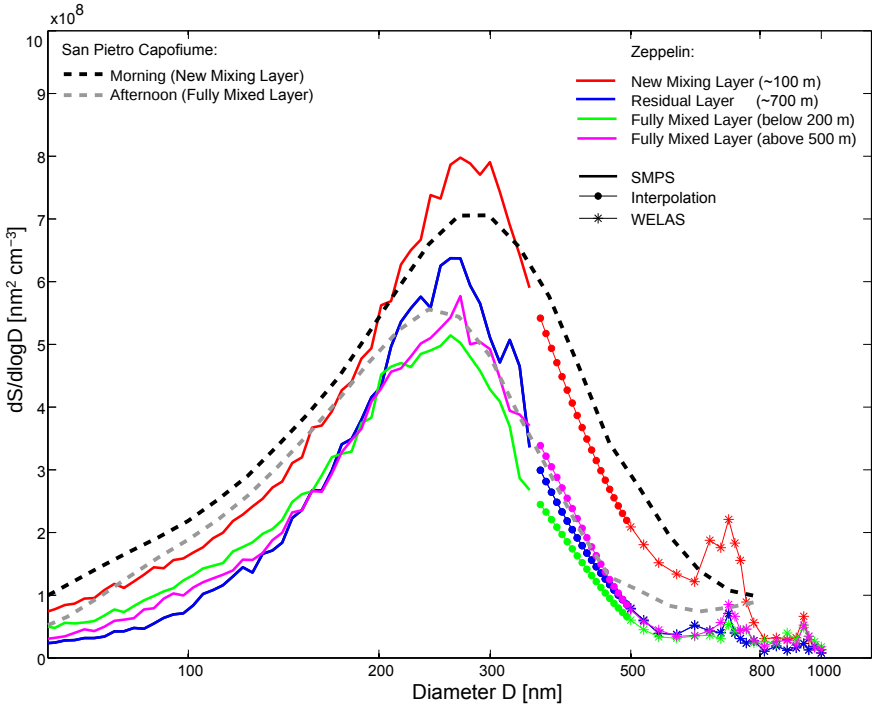

Figure 3. Dry surface area size distributions for different times and layers were probed during 20 June 2012. The colored lines denote the results measured on board the Zeppelin showing the contribution by the SMPS (straight line), WELAS (stars) and the interpolation in between (dotted line). During the early morning hours the new mixing layer (red line) and just above the residual layer (blue line) could be probed. Later during the day the results are representative for the fully mixed layer (green and pink lines for different altitudes). The dashed lines were recorded at the SPC ground stations, where the black line shows the results for the morning hours (new mixing layer~~was probed~~) and the gray line for the early afternoon (fully developed mixed layer~~was probed~~).

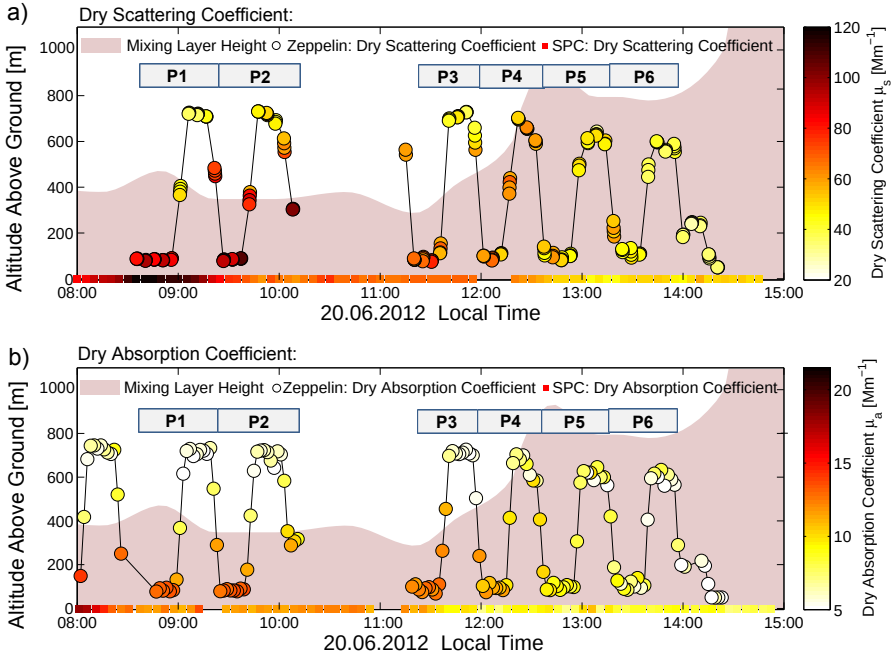

Figure 4. Time evolution of the dry scattering **(a)** and absorption **(b)** coefficients from the airborne and ground based platforms. The color scale represents the magnitude of the coefficients. The uncertainty of the dry scattering coefficients is estimated to be $\pm 18\,\%$, while $\pm 20\,\%$ is estimated for the absorption coefficients. Additionally, the ~~filled area~~ shading in **(a)** and **(b)** denotes the estimated mixing layer height (compare to the violet line in Fig. 2) and each height profile ($P1$-$P6$) is marked.

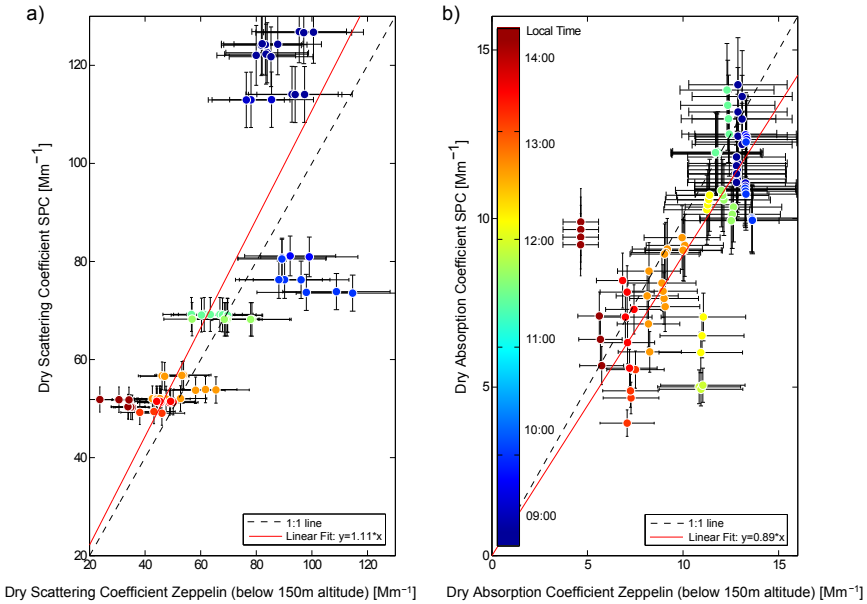

Figure 5. Comparison of dry scattering **(a)** and absorption **(b)** coefficients for ground-based and airborne measurements. The Zeppelin results were restricted to altitudes below 150 m in order to eliminate differences due to potential changes in atmospheric layers. The colors of the symbols reflect the time of the day according to the color bar in **(b)**. Additionally, the regression curves and equations are shown. **(a)** For the ground based data an uncertainty of 5 % is estimated while $\sim$ 18 % was found for the airborne calculations. **(b)** The uncertainty of the airborne absorption coefficients is estimated to be $\pm$20 %, while $\pm$13 % is estimated for the ground based results.

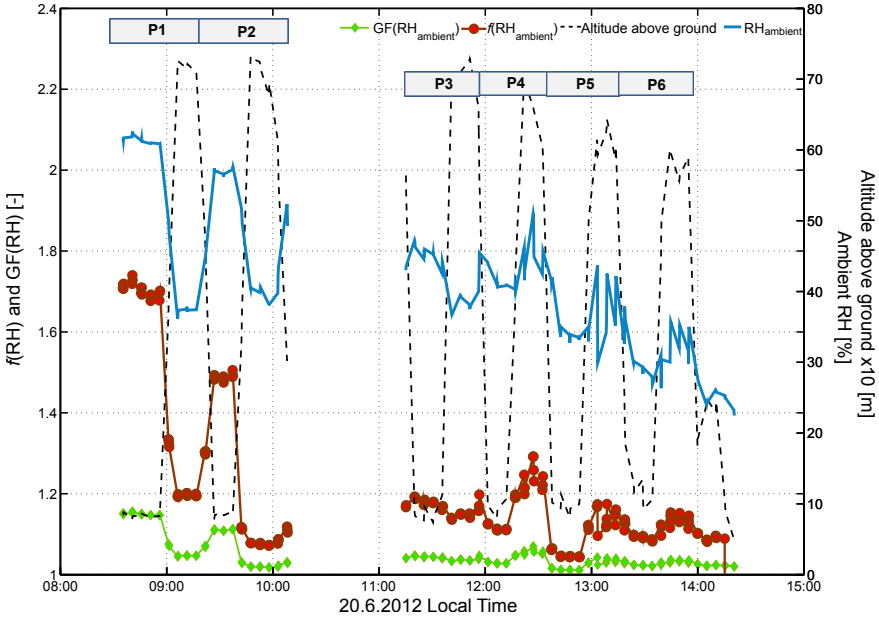

Figure 6. Time series of hygroscopic properties and ambient RH. The blue line illustrates the ambient RH ~~present~~ during the flight (right y axis). The green diamonds ~~reflect~~ show the growth factor (GF) for the ambient RH calculated from GF(RH=95 %) measurements for 500 nm particles with the WHOPS. The red line shows the scattering enhancement factor (f(RH)) during the flight as derived from the ambient RH and the GF measurements. The uncertainty of the airborne f(RH) amounts to approximately 30 %, while the GF values are expected to have uncertainties < 10 %.

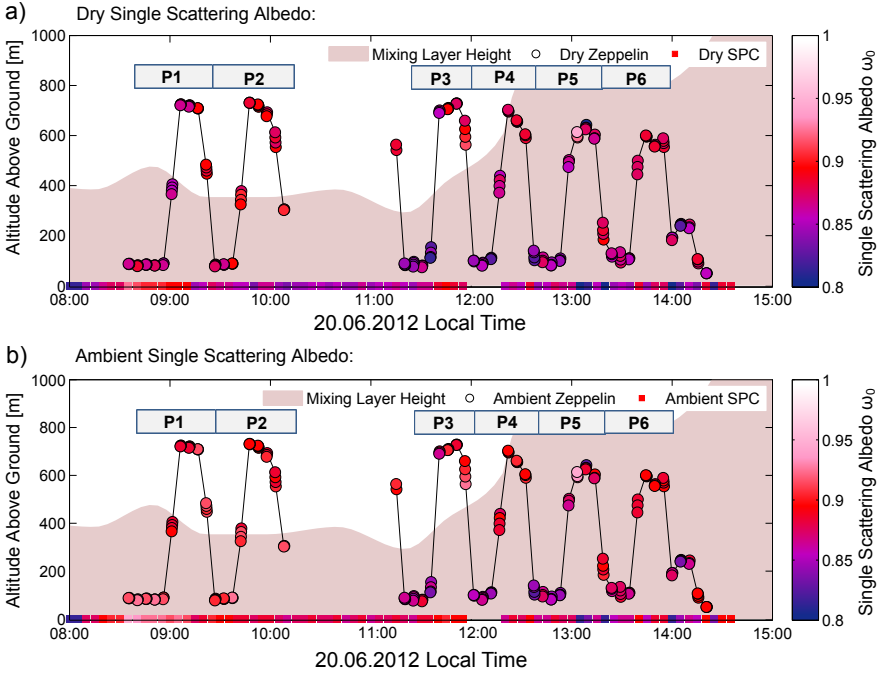

Figure 7. Time evolution of the dry **(a)** and ambient **(b)** single scattering albedo from the airborne and ground based platforms. The color scale represents the magnitude of the coefficients. The uncertainty of the dry single scattering albedo is estimated to be $\pm 7\,\%$ and $\pm 26\,\%$for SPC and the Zeppelin, respectively. The uncertainty of the ambient single scattering albedo is estimated to be $\pm 36\,\%$ and $\pm 26\,\%$ for SPC and the airborne data, respectively. Additionally, the ~~filled~~ shaded area in **(a)** and **(b)** denotes the estimated mixing layer height and each height profile ($P1$-$P6$) is marked.

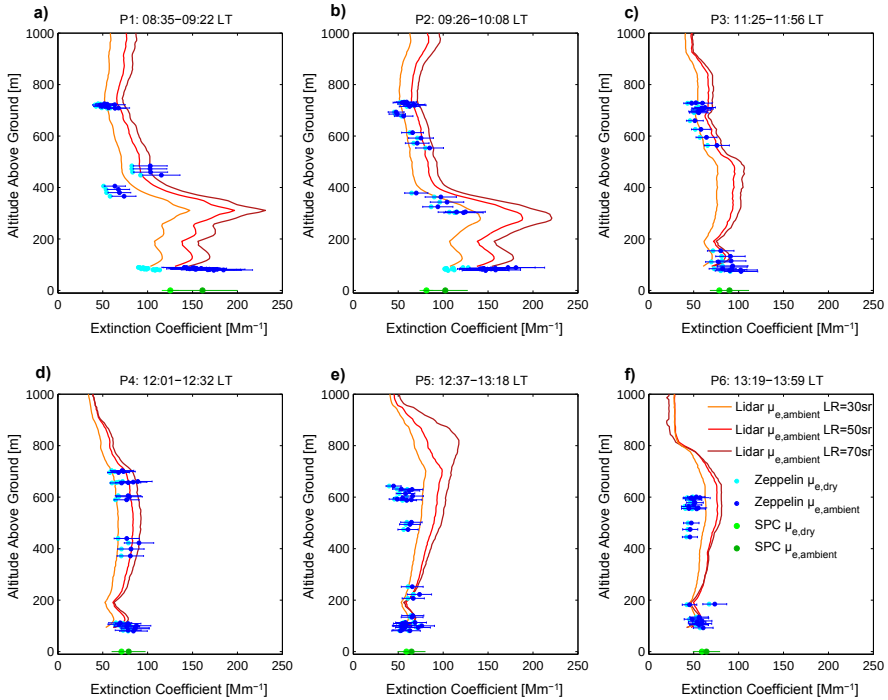

Figure 8. Extinction coefficients for profiles $P1$–$P6$ at different times of day. The lines reflect LIDAR results for assumed LRs of 30, 50 and 70 sr in orange, red and dark red, respectively. The dots describe in-situ results. In light and dark blue, dry and ambient airborne extinction coefficients are shown while the light and dark green dots represent the dry and ambient ground based results, respectively.

Supplementary Material: Ceilometer retrieval of the mixing layer height (MLH)

At the San Pietro Capofiume ground station an automated LIDAR-ceilometer (Jenoptik CHM15K “Nimbus”) was deployed to get an estimate of the mixing layer height at a certain time. The analysis is performed by manually evaluating the MLH by a skilled operator's visual analysis of three plots obtained by the pre-processing of the ceilometer signal. The data was also compared to radio sounding measurements performed at 11 UTC and vertical profiles of the potential temperature (Θ) recorded aboard the Zeppelin NT.

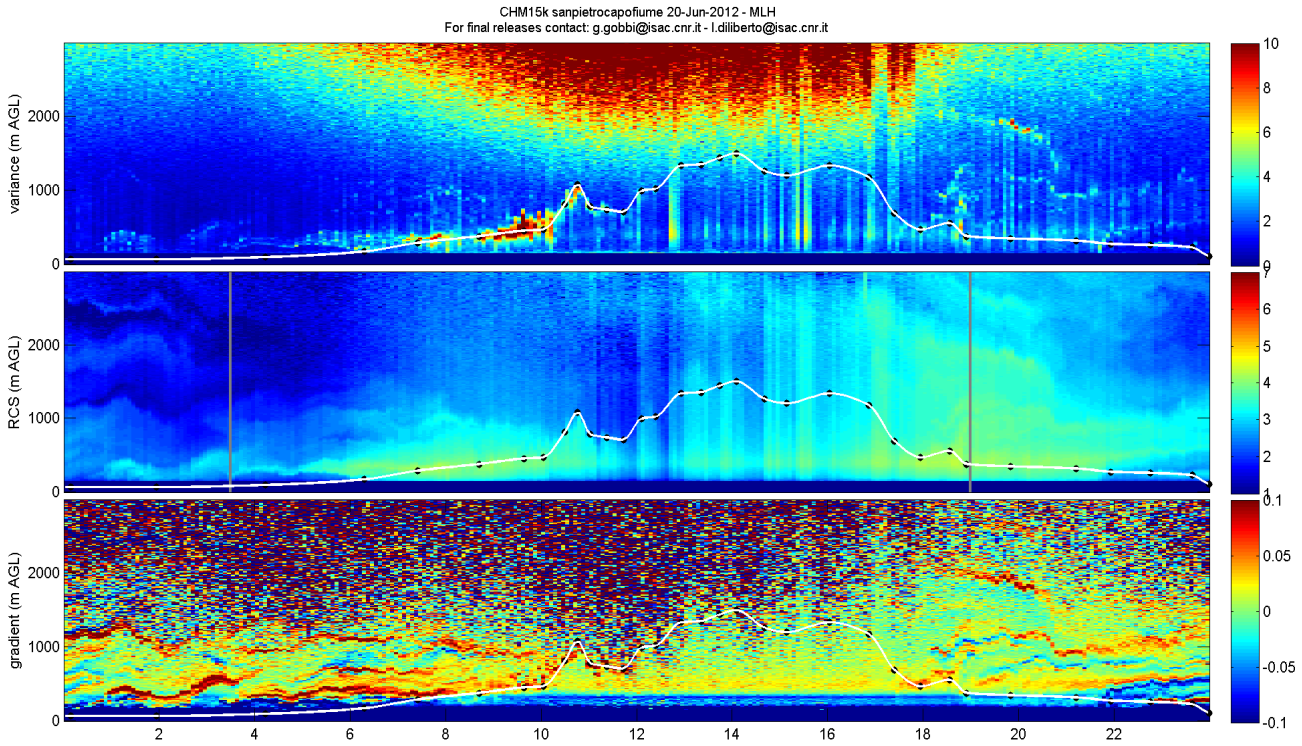

Figure 1: Three plots obtained by the pre-processing of the ceilometer signal. The white line represents the spline fit to the black dots marked by the operator while considering all the information from the three plots. The first panel illustrates the signal's variance plot (e.g. Angelini et al., 2009), the second the range corrected signal (RCS) plot and the third the signal's gradients plot.

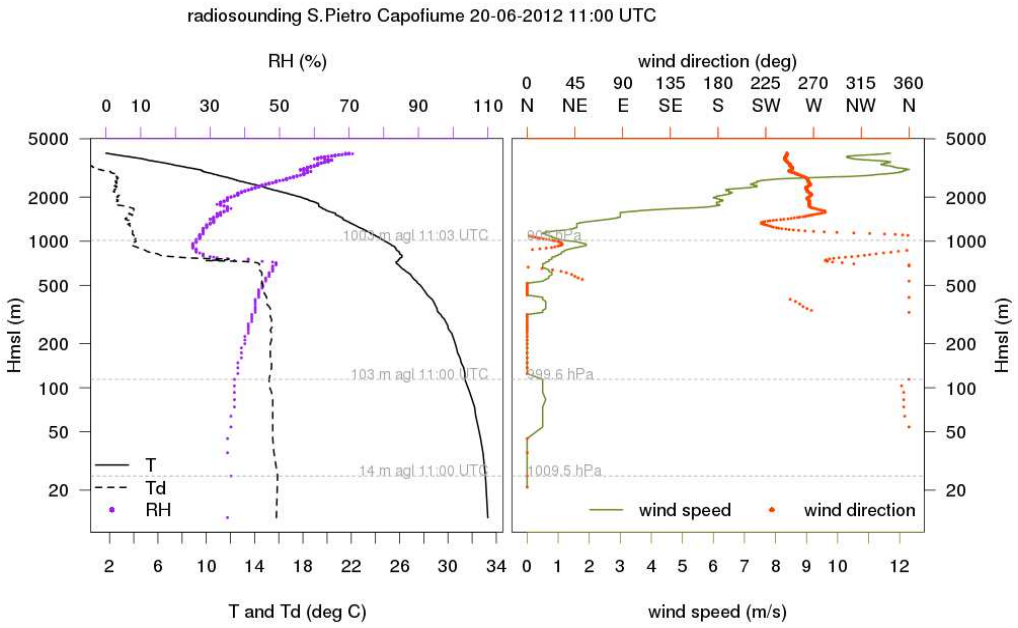

Figure 2: Radio sounding at San Pietro Capofiume at 11 UTC. The left panel illustrates the temperature T, dew point Td, and relative humidity RH as functions of altitude. The right panel shows wind speed and wind direction. The radio sounding yielded a MLH of 753 m.

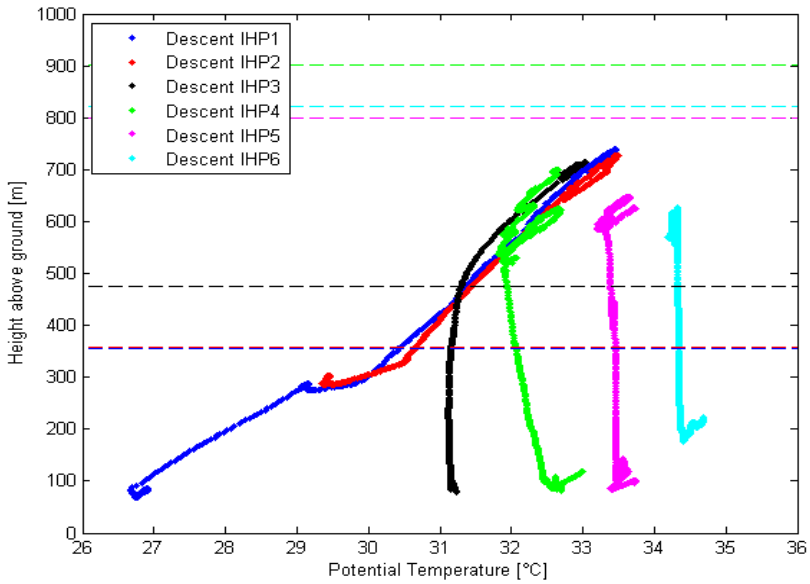

Figure 3: Height profiles of the potential temperature (Θ) measured aboard the Zeppelin NT during the flight on 20 June 2012. Each color represents the descents of height profiles 1-6 (IHP1-6), respectively. The horizontal lines depict the estimated mixed layer height (MLH) from the ceilometer retrieval during the six height profiles. A clear vertical structure of Θ is visible for the first two profiles, while the last four show very little or no altitude dependence at all. This indicates that the sub-layers in the PBL where still separated at the beginning of the flight and that a fully mixed layer was probed at the end. The estimated MLH retrieved from the ceilometer shows comparable results with a low MLH of approximately 350 m above ground in the morning that evolves to over 800 m above ground later during the day.

Supplementary Material: LIDAR data analysis

The LIDAR used in the present study is a small portable LIDAR that measures polarized and depolarized elastic backscatter. It is also equipped with an acquisition channel for detecting Raman backscattering, which is used solely to reconstruct the LIDAR signal from the lowest layer of the atmosphere, as detailed in the manuscript (partial FOV correction). The weak intensity of the Raman signal does not allow to extend the Raman profile much beyond the 2 km range maintaining a satisfactorily S/N, even if averaged over several hours at night-time, so it is not possible to use it for a Rayleigh-Raman extinction retrieval, as usually done on larger and more performing LIDAR systems. Raman profiles are thus not routinely acquired during each measurement session, but only on the occasion of LIDAR setup and alignment, for the sole scope of partial FOV reconstruction.

Lidar polarized and depolarized backscatter data are acquired in both photon counting and current mode, in two acquisition channels, every 30 s and further averaged over 600 s.

A common profile for each channel is computed by gluing the two acquisition modes in a merging region where both are considered reliable (photon counting channel far from saturation, current channel still sufficiently sensitive), generally taken between 3 and 7 km depending on light background conditions. In the particular setup of the data presented in the submitted manuscript, the gluing region was chosen above 7 km due to some unwanted noise in the photon counting acquisition mode, present in the timeframe of the campaign.

Let $S_{par}(z)$ and $S_{cross}(z)$ be the raw data of the polarized and depolarized acquisition channel respectively. In order to derive the volume depolarization DR, when it is possible to detect a region of atmosphere supposedly free of aerosol (the "calibration region" at z_0), we choose a suitable parameter K so to pose the volume depolarization DR(z),

$$DR(z)=K*(S_{cross}(z)/S_{par}(z)),$$

equal to DR_0 (the value expected for a purely molecular atmosphere) in correspondence of the z_0 region. As reported in the manuscript, the DR_0 value is assumed from literature, and depends, among other factors, on the LIDAR instrumental setup. However, there are cases when it is not possible to find such a calibration region within the useful LIDAR range, i.e. where the noise affecting the depolarized signal is deemed acceptable. In such cases, DR(z) is calculated by computing the relative gains of the two acquisition channels, retrieved from cases when a calibration region was defined. Generally, the calibration region approach works fine for night-time measurements, while the relative gain approach is used for diurnal measurements.

Correction for partial FOV overlap is made by multiplying $S_{par}(z)$ by an overlap function FOV(z) to reconstruct the signal in the lower layers of the atmosphere

$$S'_{par}(z)=FOV(z)*S_{par}(z)$$

This is displayed in Fig. 4, where the black line reports the uncorrected data, and the red line the partial FOV corrected ones.

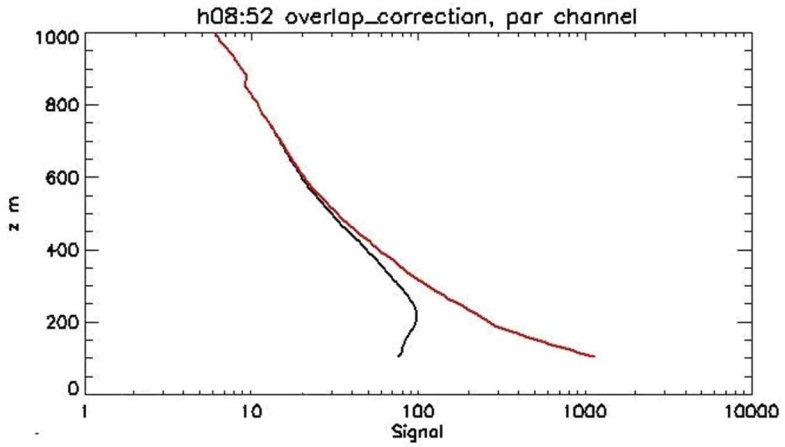

Figure 4: Profile raw $S_{par}(z)$ in black, and FOV corrected $S'_{par}(z)$ in red.

The extinction correction is made by using the molecular volume backscattering coefficient profile rho(z) as ancillary data, and iteratively choosing the parameter C to pose the total backscatter ratio R(z)

$$R(z)=C*(S'_{par}(z)*(1+DR(z))/(1+DR_0))/rho(z)$$

equal to 1 in a region of atmosphere supposedly free of aerosol. Iterations are made by computing the extinction along the profile by means of tentative R(z)s, using piecewise constant backscatter-to-extinction ratio (LR(z)) along the profile, whose values are chosen accordingly to the values of R(z) and DR(z) as detailed in the manuscript, and repeating the process until the value of R(z) remains stable between two successive iterations.

Figure 5 presents the result of such an inversion for a particular profile among those used in the analysis reported in the manuscript (8:52 UTC, 10 minutes average). It is worth noting the presence of thick layer of aerosol close to 4km, which has been identified as Saharan dust, based on its optical properties. There, LR has been fixed to the value expected for such kind of particles while elsewhere it has been fixed to values expected for polluted continental aerosol (see table 1 in the manuscript).

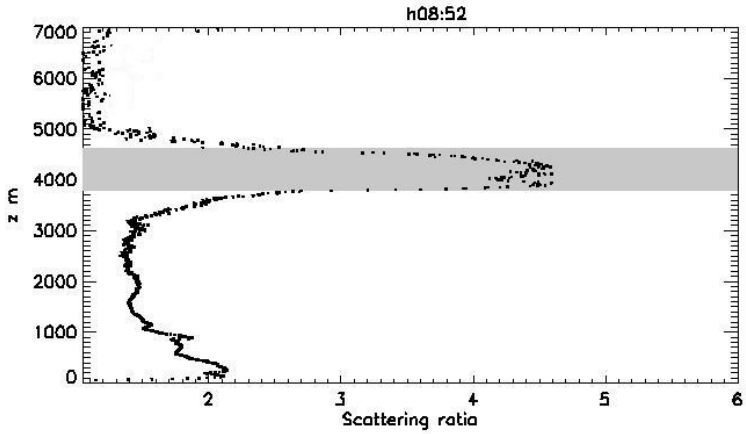

Figure 5: Scattering ratio. The grey region highlights a layer of Saharan dust.

Aerosol extinction is then computed: (z)=(R(z)-1)*rho(z)*LR(z)

In order to further support the choice of LR(z) based on the aerosol optical characteristics, we present a back trajectory study based on the Flexpart lagrangian system driven by GFS meteorological input. Back trajectories were released in correspondence of the measured profile from the 0m-2000m (Fig. 6, left panel) and 3000m-5000m (Fig. 6, right panel) vertical layers. The images show the footprint (residence time, in ns, of particles on each geographical bin) of the cluster in shaded colors and the position of the center of mass with black dots. Lower panels report the height of the center of mass during its flights backward in time.

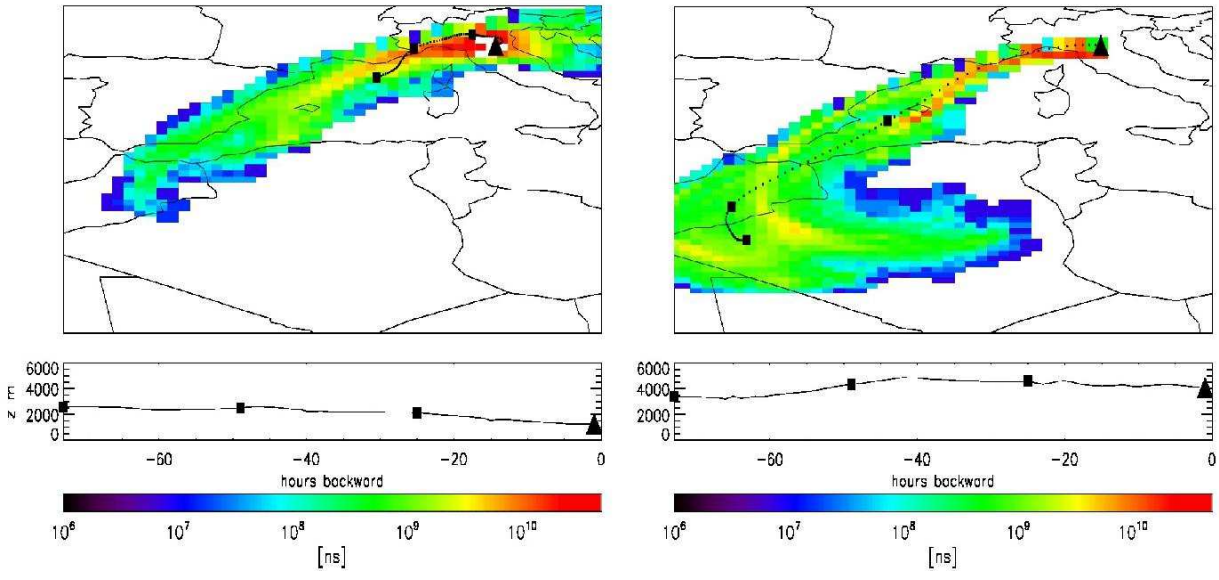

Figure 6: Flexpart footprint (in colors) and trajectories center of mass position (black dots) for the 0m-2000m release (left) and 3000m-5000m release (right). Lower panels indicate the center of mass height backward in time. Black triangle highlights the release point and black squares the mean position each 24 hours.

Figure 6 shows that, in the 0m-2000m layer, air masses are mostly influenced by local air and air coming from the sea, confirming the choice of a non – dust LR for this vertical interval. Between 3000m and 5000m heights instead back trajectories reach North Africa, involving a possible transport of Saharan particles to SPC. The identification of dust for this layer, derived by the optical parameters, is therefore also supported by the lagrangian analysis.

As pointed out in the text, changes in the assumption of LR have two consequences:
i) a "global" one on the retrieval of the backscattering coefficient profile (and the backscatter ratio profile R(z)), whose values decrease with increasing LR, the more the further down from the calibration altitude;

ii) a "local" one on the extinction retrieval, as the latter is simply linearly proportional to the backscattering coefficient, everywhere.

In order to determine the relative amount of the two counteracting effects, a sensitivity study has been performed by fixing the LR from 30 to 50 to 70 sr everywhere along the profile (irrespective of optical particle classification, to simulate the worst case). Figure 7 shows the effect of different LR choices on the backscatter ratio (left panel) and on the extinction coefficient (right panel) for one of the profiles used in the manuscript (8:52 UTC, 10 minutes average). Black, blue and red lines represent respectively the LR 30, 50, 70 sr and the black square indicates the calibration region.

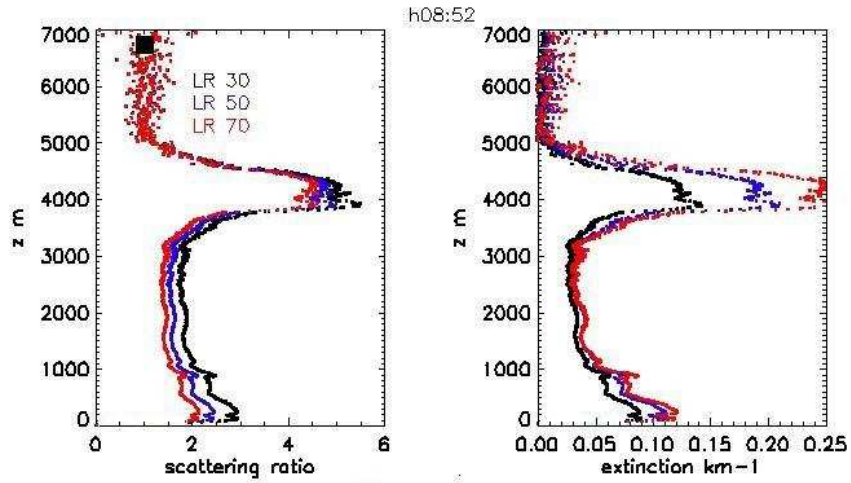

Figure 7: Left panel, Scattering ratio, right panel extinction coefficient. Red, blue and black show respectively the 70, 50 and 30 LR choice. Black square represent the calibration altitude range.

In the case studied, the "global" effect on R(z) can be clearly seen to increase the further down from the calibration altitude, not perceptible above 500m and causing a 100% variation on the aerosol scattering ratio

R(z) -1 in the PBL. As expected, the larger the LR, the smaller the R(z). This effect reverses its sign when looking at the extinction coefficient, where the “local” effect prevails, more markedly at the Saharan dust level, centered at 4 km, (100% from 30 to 70 sr), slightly less in the boundary layer (around 50% variability). A comprehensive analysis of the meteorology and transport regimes of the summer 2012 Po Valley PEGASOS campaign, associated with aerosol characterization, will be presented in Bucci et al., Transport regimes analysis over Po Valley during summer 2012: impacts on Planetary Boundary Layer variability and aerosol content, to be submitted to Atmos. Chem. Phys. Discuss